Article

Cell Host & Microbe

Chemical inhibition of a bacterial immune system

Graphical abstract

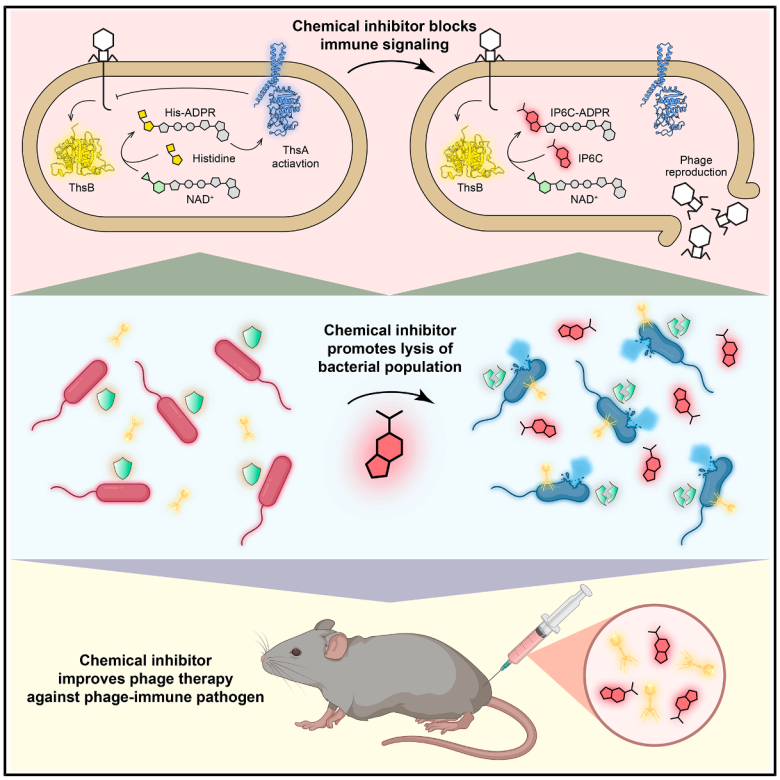

Authors

Zhiyu Zang (臧芷育), Olivia K. Duncan, Dziugas Sabonis, ..., Joseph Bondy-Denomy, Giedre Tamulaitiene, Joseph P. Gerdt

Correspondence

jpgerdt@iu.edu

In brief

Bacteriophages are promising alternatives to antibiotics for treating bacterial infections. However, bacteria possess immune systems that neutralize bacteriophages. Zang et al. discover small molecules that inhibit one such antiviral defense system, thereby resensitizing bacteria to bacteriophages in mouse infection models and complex polymicrobial communities.

Highlights

- Imidazo[1,2-*a*]pyridines selectively inhibit type II Thoeris anti-phage system
- Thoeris inhibitors halt His-ADPR production by TIR-domain protein ThsB
- Compound IP6C improves phage-therapy efficacy against *Pseudomonas aeruginosa* in mice
- IP6C is effective against Thoeris in complex polymicrobial communities

Zang et al., 2026, Cell Host & Microbe *34*, 263–277
February 11, 2026
https://doi.org/10.1016/j.chom.2026.01.003

CellPress

Cell Host & Microbe

CellPress
OPEN ACCESS

Article

Chemical inhibition of a bacterial immune system

Zhiyu Zang (臧芷育),[1,9] Olivia K. Duncan,[1] Dziugas Sabonis,[2] Iana Fedorova,[3] Yun Shi,[4,10] Gause Miraj,[4] Shuai Le (乐率),[5] Jun Deng (邓均),[5] Yuhao Zhu (朱宇豪),[5] Yanyao Cai (蔡炎尧),[1] Chengqian Zhang,[1] Garima Arya,[6] Shelley A.H. Dixon,[7] Steven P. Angus,[7] Breck A. Duerkop,[6] Haihua Liang (梁海华),[8] Robert H. Pepin,[1] Thomas Ve,[4] Joseph Bondy-Denomy,[3] Giedre Tamulaitiene,[2] and Joseph P. Gerdt[1,11,*]

[1]Department of Chemistry, Indiana University Bloomington, Bloomington, IN 47405, USA
[2]Institute of Biotechnology, Life Sciences Center, Vilnius University, Vilnius 10257, Lithuania
[3]Department of Microbiology and Immunology, University of California, San Francisco, San Francisco, CA 94158, USA
[4]Institute for Biomedicine and Glycomics, Griffith University, Gold Coast, QLD 4215, Australia
[5]Department of Microbiology, College of Basic Medical Sciences, Key Laboratory of Microbial Engineering Committee in Chongqing, Army Medical University, Chongqing 400038, China
[6]Department of Immunology and Microbiology, University of Colorado Anschutz Medical Campus, School of Medicine, Aurora, CO 80045, USA
[7]Department of Pediatrics, Herman B. Wells Center for Pediatric Research, Indiana University School of Medicine, Indianapolis, IN 46202, USA
[8]College of Medicine, Southern University of Science and Technology, Shenzhen 518055, Guangdong, China
[9]Present address: Global Health Institute, Swiss Federal Institute of Technology Lausanne (EPFL), 1015 Lausanne, Switzerland
[10]Present address: Medicinal Chemistry, Monash Institute of Pharmaceutical Sciences, Monash University, Parkville, VIC 3052, Australia
[11]Lead contact
*Correspondence: jpgerdt@iu.edu
https://doi.org/10.1016/j.chom.2026.01.003

SUMMARY

The rise of antibiotic resistance motivates a revived interest in phage therapy. However, bacteria possess dozens of anti-phage immune systems that confer resistance to therapeutic phages. Chemical inhibitors of these anti-phage immune systems could be employed as adjuvants to overcome resistance in phage-based therapies. Here, we report a class of chemical inhibitors that selectively inhibit type II Thoeris anti-phage immune systems from diverse bacteria—including antibiotic-resistant pathogens, thereby sensitizing phage-resistant bacteria to phages. These inhibitors block the biosynthesis of a histidine-ADPR intracellular "alarm" signal by ThsB, thereby preventing ThsA from arresting phage replication. Chemical inhibition of the Thoeris defense improves the efficacy of a model phage therapy against a phage-resistant clinical isolate of *P. aeruginosa* in a mouse infection, suggesting a therapeutic potential. These findings demonstrate that the selective inhibition of anti-phage defense systems can improve the efficacy of therapeutic phages, suggesting a strategy to circumvent phage-therapy resistance.

INTRODUCTION

The spread of antibiotic-resistant bacteria is one of humanity's greatest health threats.[1] Bacteriophages (viruses that infect and kill bacteria) are a promising option for treating multidrug-resistant bacterial infections.[2] However, phage resistance in pathogens is a parallel risk to antimicrobial resistance.[3] Anti-phage immune systems are already widespread across many pathogenic bacteria, limiting the lytic efficacy of phages.[4–6] We propose that small-molecule inhibitors of anti-phage systems could be co-administered adjuvants to increase the efficacy of phage therapy against phage-resistant infections. Additionally, a selective small-molecule inhibitor of an anti-phage system could "turn off" a single anti-phage defense to reveal the importance of that individual immune system for a bacterium or an entire microbial consortium within their native environments.

To identify small-molecule inhibitors of anti-phage systems, we focused on the recently discovered Thoeris system. This immune system is widespread across bacteria—including human pathogens.[7] Thoeris systems typically consist of two proteins, ThsA and ThsB. ThsB is a Toll/interleukin-1 receptor (TIR)-domain protein that produces a signal molecule after sensing phage infection[8] (e.g., by sensing phage capsid proteins[9]). The signal molecule then binds to the effector protein ThsA, which activates ThsA to arrest phage replication and/or kill the host cell before new phage progeny are produced.[8] Thoeris systems are classified into different types based on the domain structure of the ThsA protein.[7,10,11] The type I Thoeris system encodes ThsA proteins with an N-terminal SIR2 (Silent Information Regulator 2) domain and a C-terminal SLOG (SMF/DprA-LOG) domain, while ThsA proteins in type II Thoeris systems comprise N-terminal transmembrane helices and a C-terminal Macro domain (Figure 1A).[7] Although both

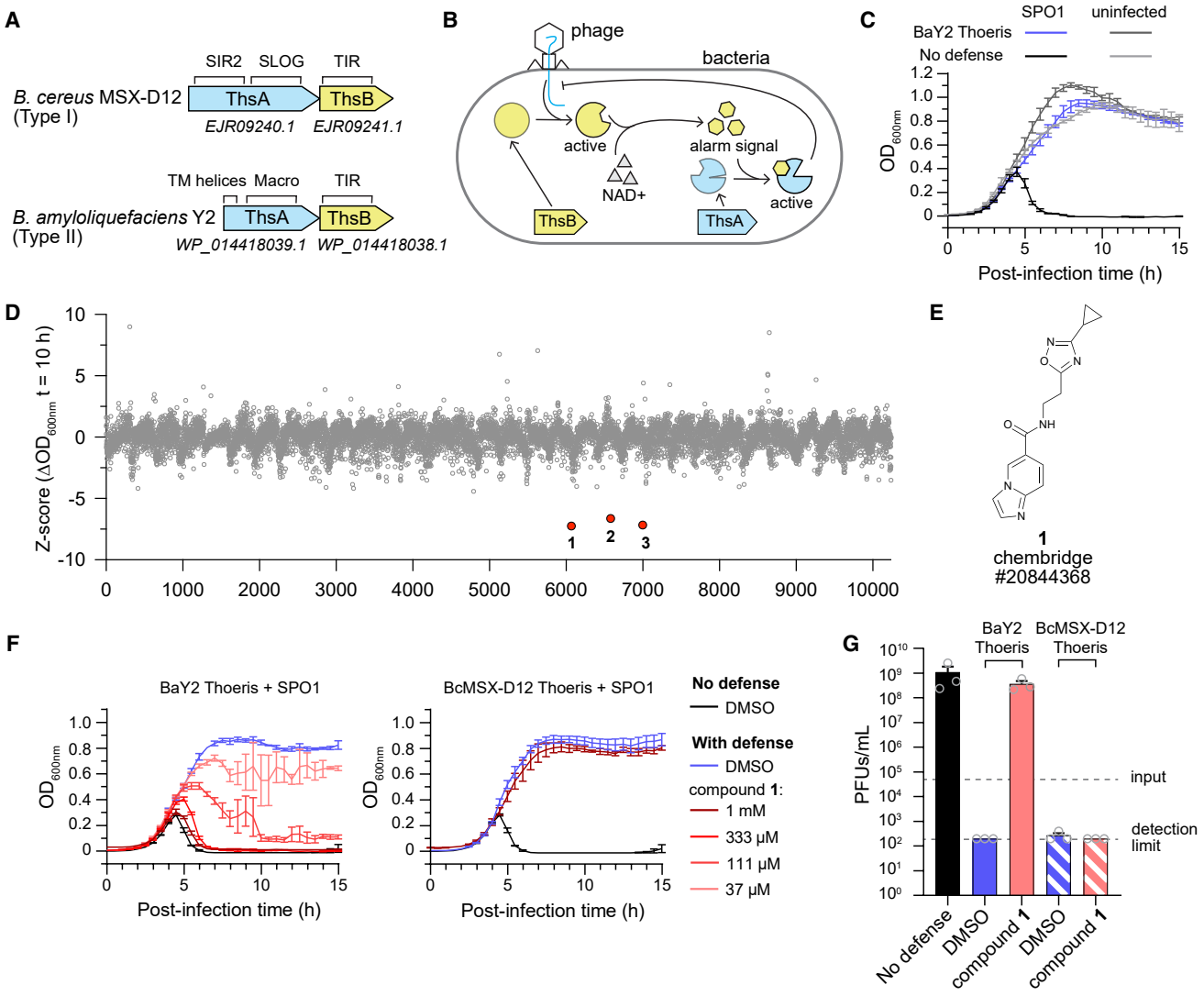

Figure 1. High-throughput screen identifies a specific inhibitor against type II Thoeris

(A) Gene composition (domain indicated above) of representative type I (*B. cereus* MSX-D12, BcMSX-D12) and type II Thoeris (*B. amyloliquefaciens* Y2, BaY2) systems.

(B) Cartoon illustrating the mechanism of defense by Thoeris systems.

(C) BaY2 Thoeris protection against phage infection, observed through improved phage-induced lysis in liquid culture. Where indicated, phage SPO1 was added at a multiplicity of infection (MOI) of 0.01. Data are represented as the average ± SEM from three independent biological replicates.

(D) *Z* score plot of the screen to identify inhibitors of type II Thoeris. The *Z* score is calculated based on the OD_{600nm} difference of the compound-treated group compared to no treatment control at 10 h post infection. The three compounds that gave significantly lower OD_{600nm} at 10 h post infection are marked red.

(E) Chemical structure of compound **1**.

(F) Compound **1** inhibited BaY2 Thoeris (type II) but not BcMSX-D12 Thoeris (type I) in liquid culture in a dose-dependent fashion, observed through improved phage-induced lysis in liquid culture. Data are represented as the average ± SEM from three independent biological replicates.

(G) Phage reproduction of SPO1, quantified by measuring the plaque-forming units (PFUs) 15 h post infection. Input indicates the initial PFUs in the culture. 1 mM of compound **1** was tested. Data are represented as the average ± SEM from three independent biological replicates. Each replicate is displayed with a gray circle.

See also Figure S1.

types of Thoeris systems encode TIR-domain ThsB proteins, it has recently been demonstrated that the two types synthesize different signal molecules.[12] In the type I Thoeris system, ThsB produces 1″-3′ glycocyclic ADP ribose (gcADPR).[13,14] This "alarm" signal then binds to the SLOG domain of type I ThsA and activates the SIR2 domain to deplete intracellular nicotinamide adenine dinucleotide (NAD^+), arresting phage replication (Figure 1B).[15] On the other hand, ThsB in the type II Thoeris system generates a histidine-ADPR conjugate (His-ADPR).[12] His-ADPR then binds to the Macro domain of type II ThsA, which triggers the oligomerization of ThsA at the cell membrane and stops phage replication.[12,16]

Moreover, two other types of Thoeris systems, type III[10] and type IV,[11] were also recently reported.

Although certain phages encode proteins that inhibit Thoeris systems,[12,13] there are not yet any examples of small molecules that inhibit Thoeris systems. Here, we discovered a class of chemical inhibitors that specifically inhibit type II Thoeris systems. These inhibitors function by blocking the production of the His-ADPR alarm signal. We found that our inhibitors can inhibit type II Thoeris systems from opportunistic pathogens. *In vivo* examination confirmed that chemical inhibition of this anti-phage defense can improve the efficacy of phage therapy in infections, suggesting a therapeutic potential of these inhibitors as adjuvants to phage therapy.

RESULTS

High-throughput screening identified an inhibitor against a type II Thoeris system

To identify chemical inhibitors of Thoeris systems, the type II Thoeris operon with its native promoter from *Bacillus amyloliquefaciens* Y2[7] (BaY2) (Figure 1A) was cloned and integrated into the genome of *Bacillus subtilis*. The presence of the BaY2 Thoeris system protected *B. subtilis* from SPO1 infection, as seen from the prevention of phage-induced host population lysis in liquid media (Figure 1C) and reduced plaque formation on solid media (Figure S1A). If a chemical were to inhibit the Thoeris system, we would expect the bacterial population to decrease over time due to phage-induced lysis, yielding a lower OD_{600nm} (optical density at 600 nm). We leveraged this measurement to perform a high-throughput screen to identify chemical inhibitors of the BaY2 Thoeris system. In a screen of 10,000 synthetic compounds, 3 molecules appeared to inhibit the BaY2 Thoeris defense and enable phage-induced host population lysis (Figures 1D and S1B). Compound **1** (Figure 1E) was validated to reproducibly help phage to lyse Thoeris-defended bacteria. As expected, this effect was dependent on the dose of compound **1** (Figure 1F) and the presence of phage (Figure S1C). However, neither compound **2** nor **3** reproduced a phage-dependent host population lysis. Compound **2** inhibited bacterial growth at a high concentration independently of phage infection (Figures S1D and S1E), while compound **3** failed to reproduce any detriment to the host bacteria (Figure S1F). Therefore, we focused on compound **1** and tested if it specifically inhibited the BaY2 Thoeris system (type II) or broadly sensitized bacteria to phages. To determine the inhibitor's selectivity, we tested if compound **1** also inhibited a type I Thoeris system from *Bacillus cereus* MSX-D12 (BcMSX-D12).[7] We cloned this Thoeris operon with its native promoter into *B. subtilis*, where it also afforded resistance to phage SPO1 (Figures 1F and S1A). Notably, compound **1** did not cause a phage-induced host population lysis in the presence of the BcMSX-D12 Thoeris system (Figure 1F). Additionally, in the *B. subtilis* host lacking any cloned defense, phage-induced host population lysis was not promoted by compound **1** compared with the DMSO control (Figure S1G). Both of these observations suggest that compound **1** is selectively a type II Thoeris inhibitor. To further confirm that the observed bacterial lysis was due to compound **1** improving phage replication, we quantified phage reproduction efficiency. As expected, both the BaY2 Thoeris system and the BcMSX-D12 Thoeris system abolished phage reproduction on *B. subtilis* (Figure 1G), and compound **1** recovered phage reproduction only on *B. subtilis* expressing BaY2 Thoeris. Besides, compound **1** failed to increase phage replication both on *B. subtilis* expressing BcMSX-D12 Thoeris (Figure 1G) and *B. subtilis* cells lacking any cloned defense systems (Figure S1H). These results strongly suggest that compound **1** is a specific inhibitor of the type II Thoeris system.

Structure-activity relationship study reveals inhibitors with improved potency

We then conducted a structure-activity relationship study on compound **1** (Figure 2A) to determine the necessary structural features for inhibition and to obtain the most potent inhibitor. To determine the essential components of compound **1**, we tested compound **4** (imidazo[1,2-*a*]pyridine-6-carboxamide, IP6C) and compound **5** (Figure 2B) for their defense inhibition activity relative to compound **1**. The inhibition of the Thoeris system was quantified by calculating the "Thoeris strength," defined as the area under the lysis curve normalized to controls[17] (Figure S2A; STAR Methods). IP6C (i.e., compound **4**, IC_{50} = 10 μM) inhibited BaY2 Thoeris more potently than compound **1** (IC_{50} = 78 μM; Figures 2C, S2B, and S2C), while compound **5** (IC_{50} > 1 mM) was inactive (Figure S2D). As expected, IP6C also promoted the reproduction of SPO1 on *B. subtilis* cells expressing BaY2 Thoeris, while compound **5** did not (Figure 2D). Therefore, IP6C is the essential portion of compound **1** to inhibit the BaY2 Thoeris system.

We next explored the electronics of the heterocycle to discern the necessary features for Thoeris inhibition. The imidazo[1,2-*a*]pyridine moiety contains a nitrogen atom at its 1-position with a lone pair of electrons that could either accept hydrogen bonds or act as a nucleophile. We hypothesized that the lone pair of electrons of N-1 could be important for the inhibition activity. To test this hypothesis, we examined Thoeris inhibition by compounds **6**–**8** (Figure 2E), in which the atom at the 1-position either possessed or lacked this lone pair of electrons. Indeed, when N-1 was changed to moieties lacking a basic lone pair of electrons [CH-1 (**6**) or NH-1 (**7**)], the inhibitors lost their activity (Figures S2E and S2F). However, compound **8**, which retained the lone pair of electrons at the N-1 position, remained active (Figure S3A). Therefore, a nitrogen at the 1-position with basic/nucleophilic electrons is essential for Thoeris inhibition.

We next asked if the imidazo[1,2-*a*]pyridine skeleton (5,6-fused bicyclic heteroaromatic) is optimal or if other sized heterocycles would be better. We tested compounds **9**–**13** (Figure 2F), which also contained a nitrogen atom with a lone pair of electrons but lacked the five-membered ring or replaced the five-membered ring with a six-membered ring. However, all adjusted skeletons were worse than IP6C (Figures S3B–S3F). Although compounds **9**–**13** share a similar skeleton with a carboxamide on the pyridine ring, only compound **9** (nicotinamide) fully inhibited the Thoeris defense (Figure S3B), albeit with lower potency than IP6C.

The carboxamide substituent location on the imidazo[1,2-*a*]pyridine skeleton could be another dictator of inhibition activity. To determine the optimal position, we tested compounds **14**–**17** (Figure 2G), which are isomers of IP6C but have the carboxamide at different positions on the imidazo[1,2-*a*]pyridine skeleton. None of the other positions showed improved inhibition compared to

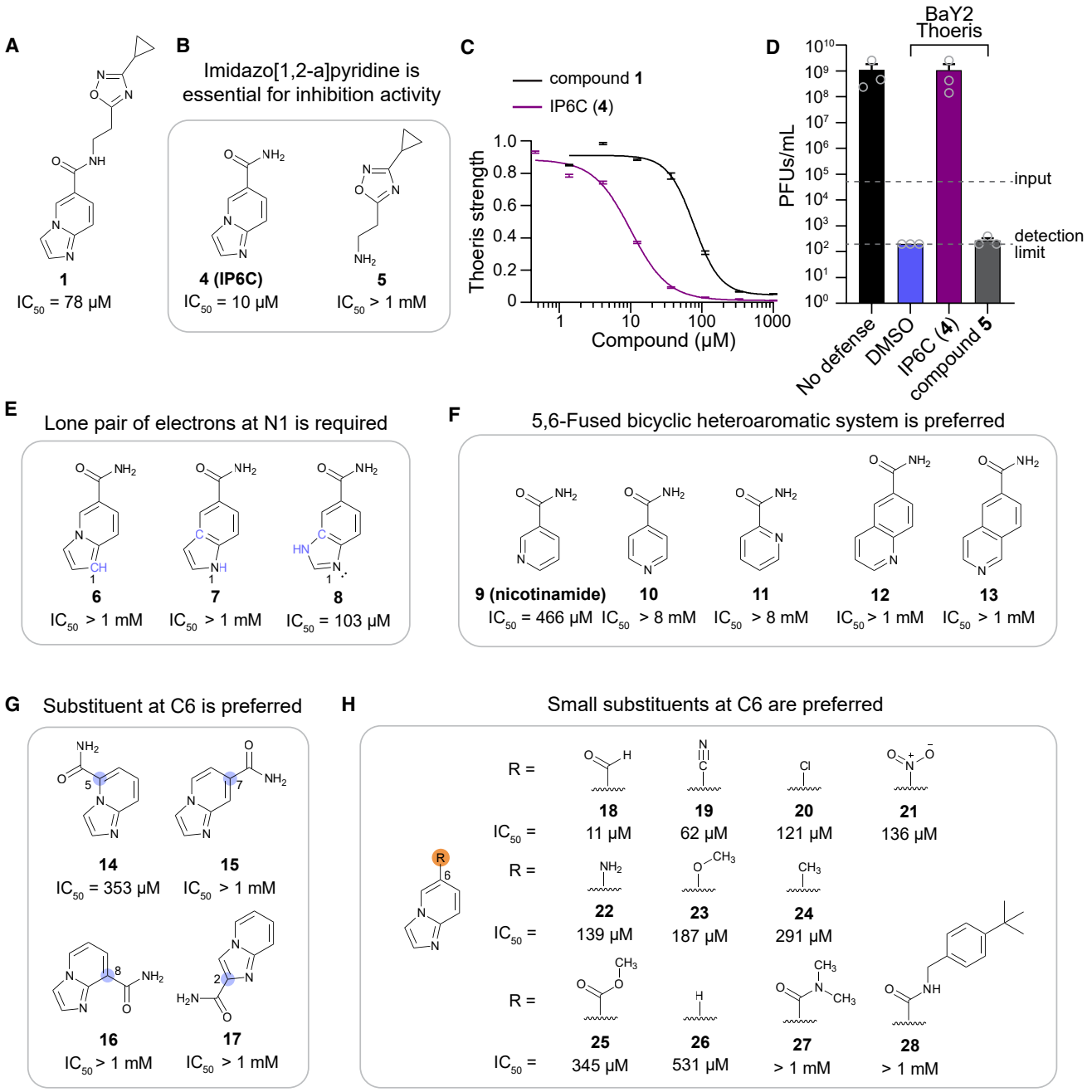

Figure 2. Structure-activity relationship study reveals optimal Thoeris inhibitors

(A) Chemical structure and IC_{50} of the initial hit (compound **1**).

(B) Chemical structure and IC_{50} of compounds IP6C (**4**) and **5**.

(C) Dose-response curve of compounds **1** and IP6C (**4**). Data are represented as the average ± SEM from three independent biological replicates.

(D) Phage reproduction of SPO1, quantified by measuring the PFUs after 15 h post infection. Input indicates the initial PFUs in the culture. 333 μM of IP6C (**4**) and 1 mM of compound **5** were tested. Data are represented as the average ± SEM from three independent biological replicates. Each replicate is displayed with a gray circle.

(E) Chemical structures and IC_{50} values of compounds **6**–**8**.

(F) Chemical structures and IC_{50} values of compounds **9**–**13**.

(G) Chemical structures and IC_{50} values of compounds **14**–**17**.

(H) Chemical structures and IC_{50} values of compounds **18**–**28**.

See also Figures S2–S6.

IP6C (Figures S4A–S4D), which suggested that the 6-position is the best location for the carboxamide substituent.

We finally evaluated a panel of compounds (**18–28**, Figure 2H) with different substituents at the 6-position. We found that small substituents at the 6-position are the most potent inhibitors (Figures S4E, S4F, S5, and S6)—possibly because steric repulsion between large substituents and the target protein's binding pocket compromises the binding affinity. An exception is the unsubstituted imidazo[1,2-*a*]pyridine (**26**): although the substituent at the 6-position (hydrogen) is the smallest among all the compounds tested, it exhibited weak potency. This observation suggests that other interactions (e.g., hydrogen bonds) between the substituent at the 6-position and the target's binding pocket are important. Therefore, the optimal structure for the inhibitor is the imidazo[1,2-*a*]pyridine skeleton with a small substituent at the C6 position.

Type II Thoeris inhibitors block production of the His-ADPR alarm signal

Phage defense by the type II Thoeris system involves two steps, each of which may be inhibited by IP6C. First, His-ADPR is produced by ThsB as an alarm signal upon sensing the phage infection.[12] Subsequently, the His-ADPR signal activates ThsA to arrest phage replication in the infected host. To test if the Thoeris inhibitors block His-ADPR production by ThsB, we constructed an IPTG-inducible (P_{spank} promoter) BaY2ThsB expression system (Figures 3A and 3B), which integrated into the *B. subtilis* genome and allowed accumulation of signal molecules for detection (as used for other immune signaling systems in bacteria[8,11–13]). When *B. subtilis* cells expressing BaY2ThsB were infected by SPO1 phages, a new peak (*m/z* = 695.1173, negative ion mode) was detected by liquid chromatography-high resolution mass spectrometry (LC-HRMS) in the cell lysate (Figures 3C and 3D), which matched the theoretical $[M-H]^-$ mass of His-ADPR. Tandem mass spectrometry (MS/MS) analysis of this peak revealed a fragmentation pattern that matched His-ADPR (Figure S7A), confirming that His-ADPR is made by BaY2ThsB upon phage infection, as reported previously.[12] The accumulation of intracellular His-ADPR was maximal 60–80 min after infection by SPO1 (Figure 3D), before cells were fully lysed by phages (~90 min post infection). We then tested if IP6C could inhibit the production of His-ADPR by ThsB after its induction with the SPO1 phage. Indeed, IP6C abolished His-ADPR production (Figures 3E and 3F), whereas its inactive analog (compound **7**, Id5C) did not (Figure S7B). The loss of His-ADPR production was not due to premature cell lysis or a general depletion of cellular metabolites by IP6C because the intracellular NAD^+ level was unchanged by IP6C treatment (Figure 3G). Repeated measurements of His-ADPR production at 80 min post infection confirmed that IP6C fully inhibited His-ADPR production in cells expressing BaY2ThsB before the cells were lysed by phages (Figures 3H and S7C). Therefore, IP6C inhibits the type II Thoeris system by blocking His-ADPR production by ThsB.

Thoeris inhibitors are competitive inhibitors of type II ThsB

The TIR domain in the ThsB proteins is known for its NAD^+ hydrolyzing activity.[16,18,19] For example, the ThsB enzyme in the BcMSX-D12 Thoeris system (type I) converts NAD^+ into 1″-3′ gcADPR.[15] It is likely that NAD^+ and histidine are the precursors of His-ADPR synthesis by ThsB in the BaY2 Thoeris system (type II).[12] TIR-domain proteins possess a conserved glutamic acid in the catalytic pocket, which is important for their NADase activity.[18,19] This glutamate (Glu99) in BaY2ThsB is essential for the anti-phage activity of the Thoeris system.[7] Therefore, we suspect that BaY2ThsB employs residue Glu99 to displace the nicotinamide from NAD^+ and form a covalent intermediate with ADPR (Figure 4A).[19] Then, a free histidine forms a covalent bond with ADPR, displacing the Glu99 residue to generate His-ADPR (Figure 4A, pathway I). Consistent with this model is our discovery that nicotinamide inhibited His-ADPR production by BaY2ThsB (Figure S7D), sensitizing bacteria to phages (Figures 2F and S2E). Since nicotinamide is proposed to be the product of the initial enzymatic step, excess nicotinamide could afford product inhibition of BaY2ThsB (Figure 4A, pathway II).

Because the imidazo[1,2-*a*]pyridine inhibitors may resemble histidine, we hypothesized that these inhibitors compete with histidine to bind BaY2ThsB, interfering with His-ADPR production. In fact, the nucleophilic N-1 atom in their heterocycles, which is necessary for inhibitory activity, might generate inhibitor-ADPR conjugates in a ThsB-catalyzed mechanism (Figure 4A, pathway III). Similar reactions exchanging heterocycle bases are catalyzed by other TIR-domain enzymes.[19] To test this hypothesis, we searched our LC-HRMS data for key evidence of inhibitor-ADPR conjugates. We examined the lysates from cells that expressed BaY2ThsB and were infected by SPO1 in the presence of IP6C. Indeed, in our prior conditions when His-ADPR production was inhibited by IP6C (Figure 3D), a new peak (*m/z* = 701.1094, negative ion mode) appeared in the cell lysate (Figure 4B). This peak matched the theoretical $[M^+-2H]^-$ mass of the hypothesized IP6C-ADPR conjugate. As further confirmation, we tested the analogous inhibitor compound **19** (IP6CN), which also inhibited His-ADPR production (Figure S7E). Similarly, a new peak (*m/z* = 683.1041, negative ion mode) appeared in the lysate (Figure S8A), matching the expected $[M^+-2H]^-$ mass of the IP6CN-ADPR conjugate. To verify the identity of the IP6C-ADPR generated in cells, we compared it with a purified IP6C-ADPR standard (Figure S8B; Table S2) generated via a reported enzyme-catalyzed base-exchange method[16] in a co-injection experiment. The IP6C-ADPR made by cells expressing BaY2ThsB co-eluted with the IP6C-ADPR standard (Figure S8C), suggesting that they are structurally identical. Therefore, IP6C is connected to the C-1″ position in ADPR through its N-1 atom (Figure S8B), as hypothesized (Figure 4A). Using the IP6C-ADPR standard as a control, we also approximated the intracellular concentration of IP6C-ADPR to be around 700 nM (1.4% of the added IP6C concentration) in the IPTG-inducible BaY2ThsB expression system (Figure S8D).

To validate that IP6C-ADPR was generated by BaY2ThsB alone, we assessed BaY2ThsB activity *in vitro*. We found that BaY2ThsB catalyzed the formation of a small amount of IP6C-ADPR from IP6C and NAD^+ over the course of an entire day (Figure 4C). This catalysis was weak because ThsB is believed to require activation by a phage component for robust activity. We also observed that IP6C-ADPR formation was facilitated by a BaY2ThsB homolog from *Agathobacter rectalis* ATCC 33656 (ArThsB, Figure S8E). The catalytically dead E99A

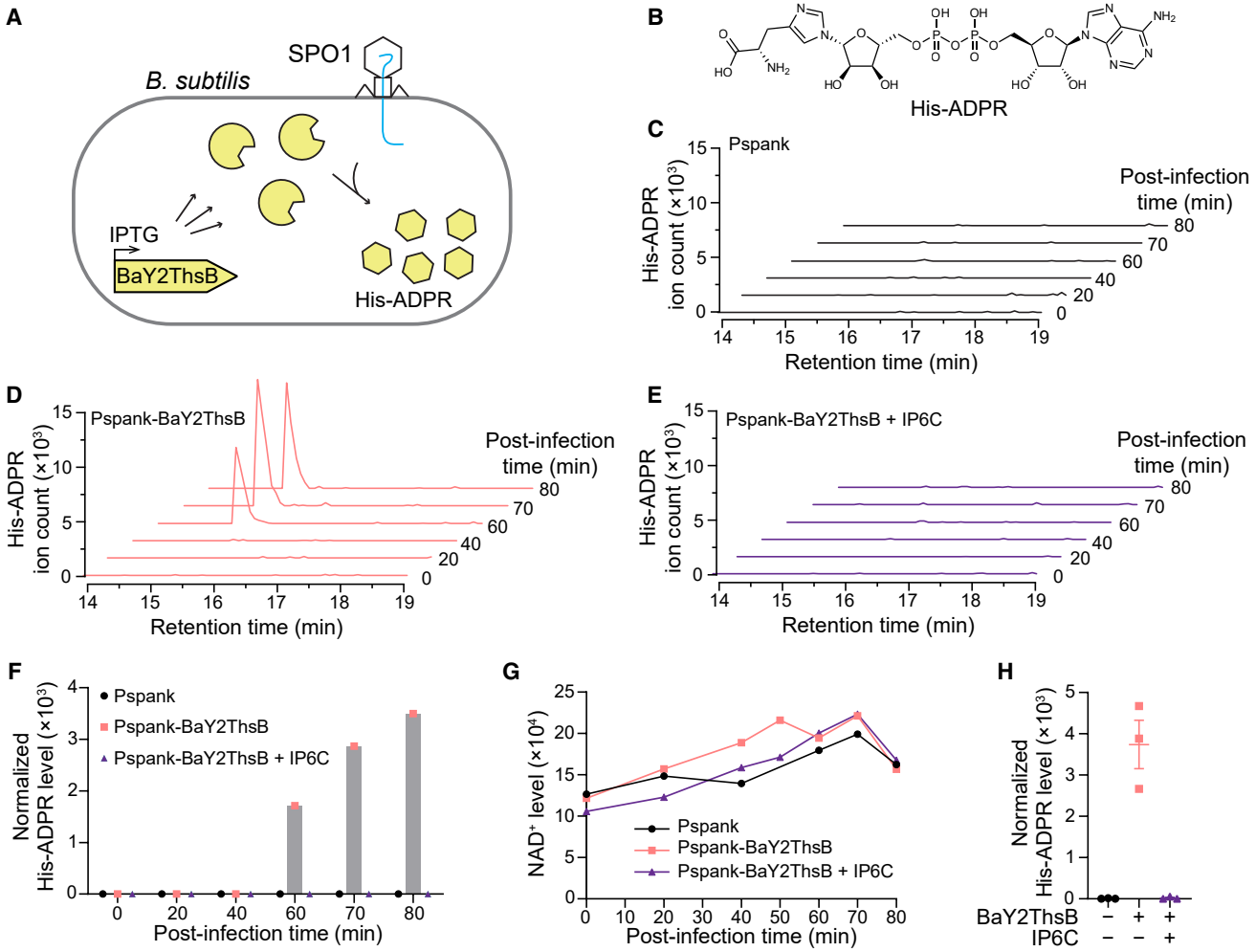

Figure 3. Production of the His-ADPR signal by ThsB is inhibited by IP6C

(A) Illustration of the production of His-ADPR by IPTG-induced BaY2ThsB upon phage infection.

(B) Chemical structure of His-ADPR.

(C–E) Extracted ion chromatogram (EIC) of His-ADPR [*m/z* 695.1169–695.1212] in the lysate of *B. subtilis* carrying (C) P_{spank} (empty vector), (D) P_{spank}-BaY2ThsB, and (E) P_{spank}-BaY2ThsB + 500 μM of IP6C.

(F) His-ADPR level (calculated as the peak area under the EIC of His-ADPR and normalized to the standard intracellular metabolite NAD^+) at different time points following SPO1 infection. 500 μM of IP6C was tested, and DMSO was used as the negative control.

(G) Intracellular NAD^+ levels reported as the peak area under the EICs of NAD^+ at each time point after SPO1 infection. 500 μM of IP6C was tested, and DMSO was used as the negative control.

(H) Biological triplicate measurement of the normalized level of His-ADPR in cell lysate 80 min after infection with SPO1. 500 μM of IP6C was tested, and DMSO was used as the negative control. Data are represented as the average ± SEM from three independent biological replicates. Each replicate is displayed with a symbol.

See also Figure S7.

mutants of both BaY2ThsB and ArThsB failed to catalyze IP6C-ADPR production (Figures 4C and S8E), further supporting our mechanistic model of IP6C-ADPR production by ThsB (Figure 4A). We also attempted to quantify the binding affinities of histidine and IP6C to ThsB. However, the weak *in vitro* activity of ThsB (Figures 4C and S8E) suggests that formation of the covalent Glu99-ADPR intermediate proceeds slowly in the absence of the yet-unknown phage activator. Consistent with this hypothesis, thermal shift assays revealed no significant binding of either histidine or IP6C to ThsB in the presence of NAD^+, as the melting temperatures remained unchanged (Figure S8F). This lack of detectable binding is likely due to the insufficient formation of the Glu99-ADPR intermediate, which is a prerequisite for histidine and IP6C interaction (Figure 4A).

Previous studies involving the human TIR-domain enzyme SARM1 (Sterile Alpha and TIR Motif Containing 1) showed that a series of heterocyclic inhibitors were "prodrugs," and the true SARM1 inhibitors were heterocycle-ADPR conjugates produced by SARM1.[19,20] We hypothesized that our imidazo[1,2-*a*]pyridine family inhibitors could also be prodrugs, and the inhibitor-ADPR conjugates produced by BaY2ThsB might be the true orthosteric inhibitors of ThsB. To test this hypothesis, we assessed if

CellPress
OPEN ACCESS

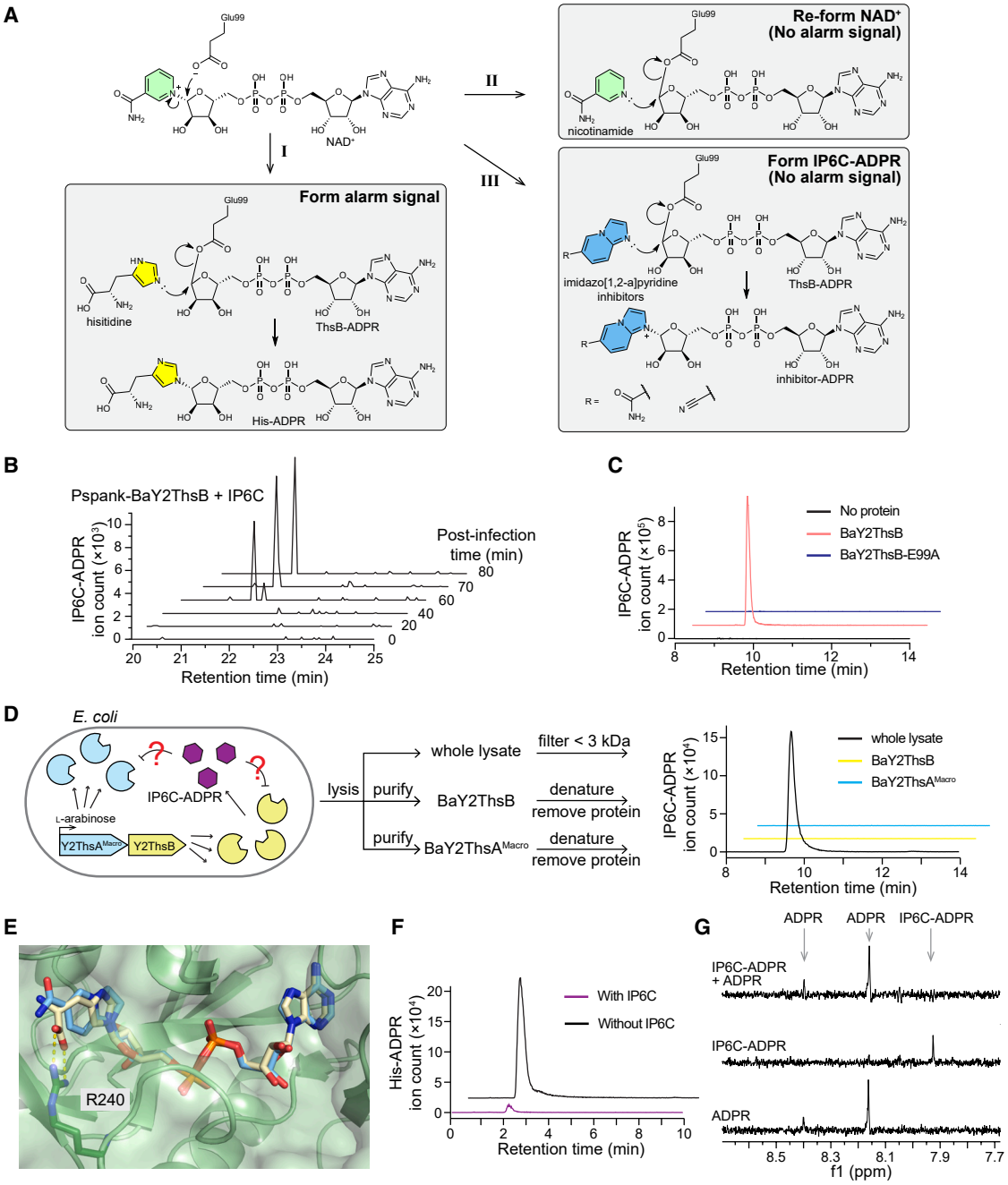

Figure 4. Thoeris inhibitors indirectly inhibit ThsA activation by competitively inhibiting His-ADPR production by ThsB

(A) Proposed mechanism of His-ADPR synthesis (I) and the inhibition mechanism of nicotinamide (II) and imidazo[1,2-*a*]pyridine inhibitors (III).

(B) EIC of IP6C-ADPR conjugate in the lysate of SPO1-infected cells expressing BaY2ThsB. Cells were cultured with 500 μM of IP6C.

(C) EIC of IP6C-ADPR in the BaY2ThsB reaction mixture. NAD^+, histidine, and IP6C were used as substrates. E99A mutation abolished the catalytic activity of BaY2ThsB.

(D) Scheme of IP6C-ADPR pull-down assay and EIC of IP6C-ADPR conjugate eluted from the BaY2ThsB and BaY2ThsA^{Macro} protein samples purified from cells grown with IP6C. Both proteins were *cis*-expressed from the same operon under the control of l-arabinose. The whole cell lysate was used as a control to verify production of IP6C-ADPR by the cells.

(E) IP6C-ADPR manually docked into BaY2ThsA Macro domain complex with His-ADPR (PDB: 8R66). The carbon atoms in the His-ADPR structure are shaded tan, and they are shaded blue in the IP6C-ADPR structure.

(legend continued on next page)

IP6C-ADPR remained bound to BaY2ThsB protein that had been purified from cells expressing BaY2ThsB in the presence of IP6C. However, although IP6C-ADPR was present in the cell lysate, it did not co-purify with BaY2ThsB (Figure 4D), suggesting that IP6C-ADPR is not a tight-binding orthosteric inhibitor of ThsB. Collectively, these results suggest that imidazo[1,2-*a*]pyridine family inhibitors are competitive inhibitors of histidine in the BaY2ThsB catalytic pocket. They cause the cell to produce inhibitor-ADPR conjugates instead of the His-ADPR alarm signal that is required to activate ThsA (Figure 4A).

Thoeris inhibitors indirectly inhibit the activation of ThsA

Since the His-ADPR alarm signal must bind to ThsA to activate its anti-phage function,[12] we hypothesized that IP6C and its analogs prevent ThsA activation indirectly by inhibiting His-ADPR production. However, we were also curious if the ThsB-produced inhibitor-ADPR conjugates had any direct impact on ThsA activation. For example, the inhibitor-ADPR conjugates could also serve as competitive inhibitors to prevent binding of low concentrations of His-ADPR to ThsA. Docking of IP6C-ADPR into the His-ADPR pocket of BaY2ThsA revealed that IP6C-ADPR fits well in the pocket and lacks interactions with R240 (Figure 4E), a residue that has recently been shown to be essential for ThsA activation.[12] Therefore, IP6C-ADPR could be a competitive inhibitor of His-ADPR binding to ThsA. To test this hypothesis, we assessed the binding of IP6C-ADPR to the ThsA Macro domain. If IP6C-ADPR binds tightly to the ThsA Macro domain, we should detect IP6C-ADPR co-purified with BaY2ThsA^{Macro}, as has been reported for His-ADPR binding to BaY2ThsA^{Macro}.[12] We co-expressed BaY2ThsA^{Macro} and BaY2ThsB in *E. coli* cells grown in the presence of IP6C. We then purified BaY2ThsA^{Macro} and attempted to detect IP6C-ADPR after denaturing the protein. As before,[21] we detected His-ADPR bound to BaY2ThsA^{Macro} in the absence of IP6C. The amount of bound His-ADPR was dramatically decreased by IP6C, presumably because it prevented the production of His-ADPR by Y2 ThsB (Figure 4F). However, no IP6C-ADPR was detected in the purified BaY2ThsA^{Macro} proteins even though IP6C-ADPR was present in the cell lysate (Figure 4D). In addition, saturation transfer difference (STD) NMR experiments also showed that IP6C-ADPR binds poorly to BaY2ThsA^{Macro} *in vitro* (Figure 4G), as bound IP6C-ADPR was completely replaced in the presence of equimolar ADPR, which itself only weakly binds the homologous ThsA from *Escherichia coli* (K_d = 4.6 ± 0.5 μM).[16] Indeed, the isothermal titration calorimetry (ITC) experiment between IP6C-ADPR and this highly conserved homolog[16] (EcThsA^{Macro}) did not reveal any interpretable binding (Figure S8G).

Although they are not definitive, our collective data strongly suggest that the inhibitor-ADPR conjugates do not bind ThsA strongly and therefore are unlikely to directly inhibit (or activate) ThsA. Instead, IP6C and its analogs indirectly inhibit the activity of ThsA by preventing the production of His-ADPR to the threshold concentration required to activate ThsA.

Thoeris inhibitors inhibit type II Thoeris systems from opportunistic pathogens

Thoeris antiviral systems are widespread in bacteria.[7] Since our inhibitors generally compete with histidine binding to ThsB, we hypothesized that these inhibitors would broadly arrest BaY2-like (i.e., type II) Thoeris systems. Most importantly, we asked if our inhibitors could block type II Thoeris systems present in human pathogenic bacterial strains that are potential targets for phage therapy (e.g., multidrug-resistant strains of *Pseudomonas aeruginosa* and *Enterococcus faecalis*, Figure 5A).[22,23] If the inhibitors work, they could resensitize these phage-resistant pathogens to phage therapy.

To study the efficacy of our Y2 Thoeris inhibitors on these homologous type II Thoeris systems, we first cloned the Thoeris operon from the antibiotic-resistant *P. aeruginosa* clinical isolate MRSN11538[24] into the genome of *P. aeruginosa* PAO1. A panel of *P. aeruginosa*-specific phages was screened against *P. aeruginosa* PAO1:Thoeris, and infection by the Lit1 phage[25] was significantly restricted by the Thoeris system (Figures 5B and S9A). Both IP6C (IC_{50} = 19 μM) and nicotinamide (IC_{50} = 185 μM) inhibited the type II Thoeris system in *P. aeruginosa*, re-enabling phage-induced host population lysis (Figures 5C, 5D, S10A, and S10B). We also tested if IP6C and nicotinamide could improve phage proliferation in the presence of Thoeris systems. Indeed, either IP6C or nicotinamide treatment allowed *P. aeruginosa* phages to propagate on hosts containing type II Thoeris defense systems (Figure 5E).

Similarly, the Thoeris operon from the antibiotic-resistant *E. faecalis* clinical isolate DS16[26] was introduced into the genome of *E. faecalis* OG1RF. After screening a panel of *E. faecalis*-specific phages, the NPV1 phage[27] was found to be susceptible to the Thoeris system (Figures 5B and S9B). As with *P. aeruginosa*, both IP6C and nicotinamide re-sensitized the Thoeris-containing *E. faecalis* to the phage. We note that these Thoeris inhibitors were less efficient against the type II Thoeris system from *E. faecalis* (Figures 5F, 5G, S10C, and S10D), exhibiting lower potencies (IP6C IC_{50} = 8.2 mM; nicotinamide IC_{50} = 1.5 mM). Despite their low potencies, IP6C and nicotinamide still fully rescued phage proliferation on Thoeris-containing hosts (Figure 5H). The lower potency of IP6C against *E. faecalis* could indicate weaker binding to the *E. faecalis* DS16 ThsB enzyme (which shares only 32% sequence identity with *B. amyloliquefaciens* Y2 ThsB). Other explanations are also plausible (e.g., IP6C may not permeate into *E. faecalis* well). Nonetheless, these results suggest that the Thoeris inhibitors can broadly inhibit type II Thoeris defenses from diverse hosts, including human pathogens.

Thoeris inhibitors sensitize a clinical pathogen to phage infection

The above experiments were performed with the PAO1 laboratory strain of *P. aeruginosa* heterologously expressing the Thoeris II defense from the MRSN11538 antibiotic-resistant clinical

(F) EIC of His-ADPR eluted from the BaY2ThsA^{Macro} protein sample purified from cells grown with and without IP6C (analogous to D), but detecting His-ADPR instead of IP6C-ADPR).
(G) Expansions of STD NMR spectra showing 10 μM BaY2ThsA^{Macro} with 1 mM ADPR (bottom), 1 mM IP6C-ADPR (middle), and 1 mM ADPR + 1 mM IP6C-ADPR (top). IP6C-ADPR signal is not observed when competing with ADPR.
See also Figure S8.

CellPress
OPEN ACCESS

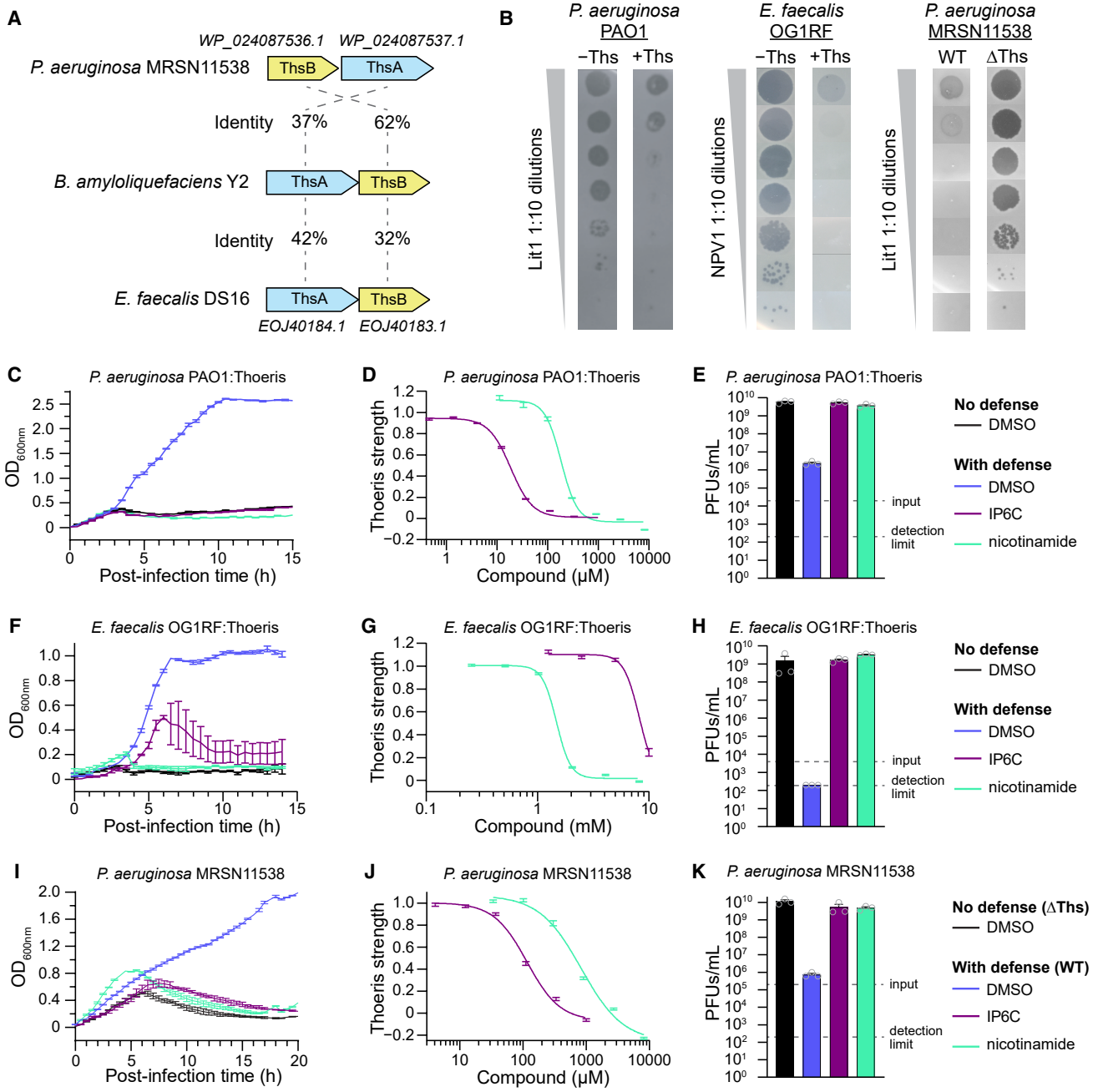

Figure 5. IP6C and nicotinamide inhibit type II Thoeris systems of antibiotic-resistant pathogens

(A) Percent identity between BaY2 Thoeris and two homologs present in antibiotic-resistant pathogens.

(B) Type II Thoeris systems protect pathogenic hosts from phage infection, observed through decreased plaquing on solid media by the phages Lit1 and NPV1. See Figure S9 for quantification of efficiencies of plaquing.

(C) IP6C and nicotinamide inhibit the *P. aeruginosa* MRSN11538 Thoeris system cloned into *P. aeruginosa* PAO1, observed through improved phage-induced lysis in liquid culture (MOI = 0.001). Data are represented as the average ± SEM from three independent biological replicates.

(D) Dose-response curves of Thoeris inhibition by IP6C and nicotinamide in *P. aeruginosa* PAO1:Thoeris. Data are represented as the average ± SEM from three independent biological replicates.

(E) Phage reproduction of Lit1 on *P. aeruginosa* PAO1:Thoeris II, quantified by measuring the PFUs 15 h post infection. Input indicates the initial PFUs in the culture. 1 mM of IP6C and 8.2 mM of nicotinamide were tested. Data are represented as the average ± SEM from three independent biological replicates. Each replicate is displayed with a gray circle.

(F) IP6C and nicotinamide inhibit the *E. faecalis* DS16 Thoeris system cloned into *E. faecalis* OG1RF, observed through improved phage-induced lysis in liquid culture (MOI = 0.001). Data are represented as the average ± SEM from three independent biological replicates.

(legend continued on next page)

isolate of *P. aeruginosa*. The utility of the inhibitor could be diminished in the true clinical isolate because its other anti-phage immune systems may afford redundant defense against the phage. To determine the importance of the Thoeris II system for phage resistance in the native MRSN11538 strain, we examined Lit1 phage infection in both this wild-type (WT) isolate and its Thoeris knockout strain. We first noticed that Lit1 only poorly infected *P. aeruginosa* MRSN11538 WT, presumably due to the presence of the Thoeris II system (Figures 5A, 5B, and S9C). Furthermore, the Lit1 phage titer increased 10^5-fold after knocking out the native Thoeris II system (Figures 5B and S9C). Since this deletion made the clinical isolate equally susceptible as the PAO1 strain to the Lit1 phage (Figures S9A and S9C), the Thoeris II system is likely to be sufficient for the full Lit1 resistance in the MRSN11538 WT strain.

Reassured by the genetic knockout, we evaluated the ability of IP6C and nicotinamide to sensitize the clinical isolate to phage. Both IP6C (IC_{50} = 116 μM) and nicotinamide (IC_{50} = 838 μM) sensitized MRSN11538 WT to Lit1 infection, leading to phage-induced host population lysis as observed in MRSN11538 ΔThoeris (Figures 5I, 5J, S10E, and S10F). Furthermore, the IP6C or nicotinamide treatment allowed Lit1 phages to successfully propagate on the MRSN11538 WT strain as in the MRSN11538 ΔThoeris strain (Figure 5K). Overall, these results suggest that IP6C and nicotinamide are powerful chemical tools that can sensitize even clinical pathogens to phage infection.

Thoeris inhibition improves the efficacy of a model phage therapy

To evaluate the therapeutic potential of Thoeris inhibitors, we tested the ability of IP6C to improve the efficacy of a model phage therapy. We hypothesized that IP6C could improve the survival rate of mice undergoing phage therapy against phage-resistant *P. aeruginosa* containing the type II Thoeris system. In brief, mice were infected intraperitoneally with Thoeris-containing *P. aeruginosa*, followed by intraperitoneal addition of Lit1 phage alone or in combination with IP6C. Survival of mice was assessed for 7 days.

In an initial test, the PAO1:Thoeris strain was used, and phage and IP6C were added immediately after bacterial infection. IP6C was also re-administered after 12 and 24 h. As a negative control, an inactive analog of IP6C (Id5C, Figure S11A) was administered in place of IP6C. The IP6C treatment improved the survival rate of mice relative to the negative control (71% [5 out of 7] vs. 29% [2 out of 7]). The increased survival rate was dependent on phage, as all mice died within one day in the group treated with IP6C only (Figure S11B).

In the second test, the antibiotic-resistant clinical isolate *P. aeruginosa* MRSN11538 WT was used. In this case, the Lit1 phage and IP6C inhibitor were administered 1 h following the intraperitoneal infection, and the mice only received a single intraperitoneal dose of Lit1 phage adjuvanted with IP6C inhibitor (Figure 6A). Again, we used the inactive analog Id5C (Figure S11A) as a negative control. The combined action of phage and IP6C treatment drastically improved the survival rate of mice to 86% (6 out of 7 survived) compared to controls in which no more than 14% (1 out of 7) animals survived (Figure 6A). Furthermore, the IP6C inhibitor was not toxic to mice (Figures S11C–S11E) or human cell lines (Figures S11F–S11K), which supports its therapeutic potential as an adjuvant in phage therapy. Mice treated with IP6C did initially eat less and lose weight, though, suggesting an opportunity to develop more selective inhibitors in the future (Figures S11D and S11E). Moreover, IP6C does not appear to negatively impact the titer of the Lit1 phage in storage (Figure S11L), suggesting that the phage and the inhibitor could be stored together as a single solution. The results of this preliminary infection model suggest that IP6C (and likely other inhibitors of anti-phage immune systems) could resensitize phage-resistant bacteria to phage therapies that would otherwise be ineffective.

Thoeris inhibitor IP6C is effective and selective in model polymicrobial community

Considering the polymicrobial nature of many clinical infections in humans,[28] we asked if IP6C can specifically target Thoeris-containing microorganisms in a complex community. We made a three-microbe mixture of common bacteria found in cystic fibrosis (based on prior work by Jean-Pierre, O'Toole, and colleagues[29]), including *Staphylococcus aureus* USA300, *Streptococcus sanguinis* SK36, and our Thoeris-containing strain of *P. aeruginosa* PAO1. We tested if IP6C could resensitize PAO1:Thoeris II to Lit1 phage and significantly decrease the PAO1:Thoeris colony-forming units (CFUs) present in the mixture. Indeed, the presence of both IP6C and Lit1 decreased the titer of PAO1:Thoeris by more than 100-fold relative to conditions that lacked IP6C, Lit1, or both (Figure 6B). IP6C was also selective—the *S. aureus* and *S. sanguinis* CFUs were unaffected (Figure 6B). Finally, we evaluated the temporal stability of IP6C within polymicrobial communities, since long-term compound integrity is essential for clinical translation. Liquid chromatography-tandem mass spectrometry (LC-MS/MS)

(G) Dose-response curves of Thoeris inhibition by IP6C and nicotinamide in *E. faecalis* OG1RF:Thoeris. Data are represented as the average ± SEM from three independent biological replicates.

(H) Phage reproduction of NPV1 on *E. faecalis* OG1RF:Thoeris was quantified by measuring the PFUs 15 h post infection. Input indicates the initial PFUs in the culture. 10 mM of IP6C and 8.2 mM of nicotinamide were tested. Data are represented as the average ± SEM from three independent biological replicates. Each replicate is displayed with a gray circle.

(I) IP6C and nicotinamide inhibit the Thoeris system in the *P. aeruginosa* MRSN11538 clinical isolate, observed through improved phage-induced lysis in liquid culture (MOI = 0.01). Data are represented as the average ± SEM from three independent biological replicates.

(J) Dose-response curves of Thoeris inhibition by IP6C and nicotinamide in *P. aeruginosa* MRSN11538. Data are represented as the average ± SEM from three independent biological replicates.

(K) Phage reproduction of Lit1 on *P. aeruginosa* MRSN11538, quantified by measuring the PFUs 20 h post infection. Input indicates the initial PFUs in the culture. 1 mM of IP6C and 8.2 mM of nicotinamide were tested. Data are represented as the average ± SEM from three independent biological replicates. Each replicate is displayed with a gray circle.

See also Figures S9 and S10.

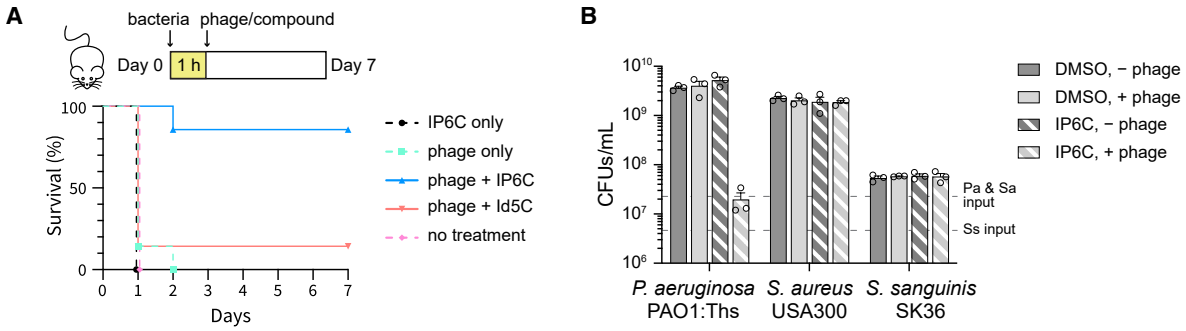

Figure 6. IP6C promotes model phage therapy in mice and in polymicrobial community

(A) Survival of 7-week-old BALB/c mice (n = 7) following intraperitoneal injection with *P. aeruginosa* MRSN11538 WT. 1 h after infection, the mice received one intraperitoneal dose of IP6C (1 mg, ∼50 mg/kg), Lit1 phage (MOI = 10), or a combination of the two. Id5C (1 mg, ∼50 mg/kg) was used as a mock control.

(B) CFUs of *P. aeruginosa*, *S. aureus*, and *S. sanguinis* in the co-culture experiment. Lit1 phage at an MOI of 0.0001 (to *P. aeruginosa*) and/or 300 μM of IP6C were added. Data are represented as the average ± SEM from three independent biological replicates. Each replicate is displayed with a black circle.

See also Figure S11.

analysis after 24 h in the co-culture setting revealed no measurable decrease in IP6C levels (Figures S11M and S11N). In fact, a slightly higher concentration was present in the culture after 24 h—likely due to evaporation of the culture and/or slight variation in sampling volumes. Therefore, IP6C appears to retain efficacy in polymicrobial environments, and it appears to have no fitness impact on other bacteria. These findings suggest that it can be an effective and selective tool to resensitize Thoeris-containing bacteria to phages in complex natural environments, including animal infections.

DISCUSSION

We discovered a class of imidazo[1,2-*a*]pyridine derivatives that inhibits type II Thoeris systems by blocking His-ADPR production by ThsB. This finding demonstrates that anti-phage systems can be selectively inhibited by small molecules, sensitizing phage-resistant bacteria to phages. Our inhibitors arrest type II Thoeris systems in multiple bacterial species, including two multidrug-resistant opportunistic pathogens. One inhibitor improved the survival rate of mice that received phage-therapy treatment to combat a phage-resistant strain of *P. aeruginosa*. Therefore, this class of inhibitors may hold future application as a therapeutic adjuvant to increase the efficacy of phage therapy against phage-resistant infections.

We note that type II Thoeris is only one of many anti-phage defense systems that can frustrate phage-based interventions. For example, the *P. aeruginosa* MRSN11538 strain in our study is predicted to have about a dozen anti-phage defenses.[30] Furthermore, Thoeris defenses are only present in 3.4% of sequenced prokaryotes.[31] Therefore, this discovery of chemical inhibitors to a single anti-phage defense will not broadly sensitize all pathogens to all phages. However, this work is a blueprint for how a high-throughput screening approach can be readily applied to target any of the dozens of other phage-defense systems.[4] In the coming years, selective inhibitors will be developed and applied against many of the most important known anti-phage immune systems. In fact, we have inhibited six other defenses in forthcoming work. Like type II Thoeris, many anti-phage systems rely on small-molecule signaling (mostly nucleotide derivatives),[32] such as type I Thoeris,[8,15] type III CRISPR,[33–35] CBASS,[36,37] and PYCSAR.[38] Among these systems, the catalytic sites of signal-synthesizing enzymes and the signal-binding sites of the effector proteins should provide deep cavities that are favorable for binding small-molecule inhibitors. On the other hand, many other anti-phage systems function through protein-protein interactions or protein-nucleic acid interactions (e.g., restriction-modification systems,[39] CRISPR-Cas systems,[40] Gabija,[41,42] Hachiman,[43] and Zorya[44]). These types of interactions involving large interfaces (1,000–2,000 Å^2 per side) are recalcitrant to inhibition by small molecules but have recently proven to also be "druggable."[45,46] For example, *in vitro* inhibitors have been developed against a CRISPR-Cas system, although they have no efficacy within bacterial cells.[47,48] We hypothesize that chemical inhibitors will exist for many, if not all, of the anti-phage systems. Each new inhibitor will expand the potential of phage therapy to target diverse phage-resistant infections. One day, any clinical isolate may be rapidly screened against a panel of phage + defense inhibitor combinations to discover the optimal treatment plan.

Beyond the therapeutic potential of phage-defense inhibitors, they could also be useful chemical tools to dissect the importance of individual defense systems in shaping microbial communities. Many bacteria harbor multiple anti-phage systems, and the importance of each system for resistance to phages is not yet clear.[49] To answer this question, selective inhibitors could easily turn off individual defenses to reveal the importance of each for phage resistance, even in genetically-intractable bacteria. Furthermore, in microbial communities, the complex benefit/cost tradeoff of harboring anti-phage immune systems[50] promotes frequent gain and loss of anti-phage systems in individual bacteria.[51] This constant flux of defense systems within microbial communities creates a "pan-immunity" to combat diverse phage predators and shape the composition of multi-species communities.[52] Selective inhibitors of anti-phage systems could be easily employed to reveal the importance of individual defense systems to the pan-immunity of complex microbial communities. For example, an inhibitor can switch off all type II Thoeris systems harbored by any member within a natural polymicrobial community,

and the subsequent change in community composition would reveal the importance of that defense for community structure in the presence of native phages. As the collection of available inhibitors increases, a microbial population could be screened with a panel of inhibitors to quickly determine which defenses are lynchpins of the community's structure. We note the challenges associated with developing potent and specific chemical inhibitors that function effectively in complex microbial communities, as exemplified by inhibitors targeting the human gut microbiome.[53] Nonetheless, the efficacy and selectivity of IP6C in polymicrobial and *in vivo* phage-therapy models underscore its promise as a lead compound for future medicinal chemistry development.

Finally, besides finding synthetic Thoeris inhibitors, we discovered that a natural metabolite (nicotinamide) inhibits ThsB as well. This observation intersects with previous work showing that microbial natural products can either sensitize nearby competitors to phage lysis[54] or provide improved resistance against phages.[55] Similarly, our finding suggests that a microbe that secretes nicotinamide or nicotinamide-containing analogs[56,57] may sensitize Thoeris-containing competitors to phages. A nicotinamide-rich host environment may also preclude the effectiveness of Thoeris-based immunity. Perhaps the conditional efficacy of Thoeris (and other defenses) in certain metabolic environments is one reason why bacteria tend to maintain multiple immune systems.[49,58]

In conclusion, we discovered a class of chemical inhibitors that can inhibit type II Thoeris anti-phage immune systems by preventing the synthesis of alarm signals. We demonstrated that these inhibitors work against the type II Thoeris systems encoded by multiple bacteria species, including two multidrug-resistant opportunistic pathogens. Notably, the inhibitor IP6C is also effective *in vivo*, where it improved phage-therapy efficacy in a *P. aeruginosa*-infected mouse model. We expect that similar efforts will provide inhibitors against dozens of other known anti-phage systems, expanding the scope of infections that can be treated with phages. We further anticipate that selective inhibitors will be valuable chemical tools to study the importance of individual anti-phage systems in complex microbiomes.

Limitations of the study

We note that the potency of both inhibitors (IP6C and nicotinamide) decreased in the clinical isolate of *P. aeruginosa* compared with the heterologous expression system in the model PAO1 strain. This reduction in efficacy may represent a general challenge when applying inhibitors to clinical isolates. Inhibitor analogs with improved potency and permeability should therefore be explored in future work. More potent inhibitors should also be administered at lower concentrations, potentially mitigating the observed weight loss in mice.

Although the Thoeris family is relatively widespread—being present in 298 different species—it is not among the most prevalent defense systems encoded in bacterial genomes.[31] Overall, Thoeris accounts for 3.4% of all identified defenses, with type II Thoeris representing 41.4% (332 out of 801) of all Thoeris occurrences. The large diversity of defense systems, each represented in only a small fraction of bacteria, underscores the need to continue developing a comprehensive library of validated inhibitors targeting distinct bacterial defense mechanisms.

Because ThsB is minimally active *in vitro* without its yet-unknown phage-induced activating conditions, classic inhibitor-binding and enzyme kinetics assays were not feasible in this study. Once these conditions are realized, the affinity of IP6C-ThsB interactions can be fully quantified.

Finally, only female mice were included in the phage-therapy experiments. Further studies will be needed to comprehensively evaluate the effects of the inhibitor-phage combination therapy, including potential sex-dependent differences and infection with complex microbial colonization.

RESOURCE AVAILABILITY

Lead contact

Requests for further information and resources should be directed to and will be fulfilled by the lead contact, Joseph P. Gerdt (jpgerdt@iu.edu).

Materials availability

All unique/stable reagents generated in this study are available from the lead contact with a completed materials transfer agreement.

Data and code availability

All data reported in this paper will be shared by the lead contact upon request.

This paper does not report original code.

Any additional information required to reanalyze the data reported in this paper is available from the lead contact upon request.

ACKNOWLEDGMENTS

We thank Jonathan Trinidad (Indiana University) for support with LC-MS/MS experiments. We thank the Bacillus Genomic Stock Center (Ohio State University) for providing bacteria and phages. We thank Tamim Mosaiab and Veronika Masic for support with NMR experiments and protein production. We thank Audrone Ruksenaite (Vilnius University) for conducting the MS experiments. The research was supported by a research starter grant from the American Society of Pharmacognosy to J.P.G., a National Science Foundation CAREER award (IOS-2143636) to J.P.G., a Camille Dreyfus Teacher-Scholar Award (TC-24-028) to J.P.G, and a National Institutes of Health grant (R35GM138376) to J.P.G. Research support was also provided by the National Health and Medical Research Council (Investigator Grant 1196590 to T.V.), the Australian Research Council (Future Fellowship FT200100572 to T.V.), a Discovery Early Career Researcher Award (DE250101258 to Y.S.), the National Institutes of Health (R01AI141479 to B.A.D.), the National Key Research and Development Program of China (2021YFA0911200 to S.L.), the Research Council of Lithuania (LMTLT) agreement no. S-MIP-24-84 (to G.T.), and the Kleberg Foundation (to J.B.-D.). Z.Z. was supported in part by the John R. and Wendy L. Kindig Fellowship. The Laboratory for Biological Mass Spectrometry was supported by the Indiana University Precision Health Initiative. The 600 MHz spectrometer of the Indiana University NMR facility was supported by NSF grant CHE-1920026, and the Prodigy probe was purchased in part with support from the Indiana Clinical and Translational Sciences Institute, funded in part by NIH Award TL1TR002531. The triple quadrupole LC-MS/MS system was generously donated by Shane Tichy of Agilent Technologies.

AUTHOR CONTRIBUTIONS

Conceptualization, Z.Z. and J.P.G.; methodology, Z.Z., S.P.A., B.A.D., S.L., T.V., J.B.-D., G.T., and J.P.G.; investigation, Z.Z., O.K.D., D.S., I.F., Y.S., G.M., S.L. J.D., Y.Z., Y.C., C.Z., G.A., S.A.H.D., and R.H.P.; visualization: Z.Z., I.F., T.V., G.T., J.P.G., and S.A.H.D.; writing—original draft, Z.Z. and J.P.G.; writing—review & editing, Z.Z., O.K.D., D.S., I.F., S.L. B.A.D., T.V., J.B.-D., G.T., and J.P.G.; funding acquisition, S.L., B.A.D., T.V., J.B.-D., G.T., and J.P.G.; supervision, S.L., S.P.A., B.A.D., H.L., T.V., J.B.-D., G.T., and J.P.G.

DECLARATION OF INTERESTS

J.B.-D. is a scientific advisory board member of SNIPR Biome, Excision BioTherapeutics, and LeapFrog Bio; consults for BiomX; and is a scientific advisory board member and co-founder of Acrigen Biosciences and ePhective Therapeutics. The Bondy-Denomy laboratory received research support from Felix Biotechnology.

STAR★METHODS

Detailed methods are provided in the online version of this paper and include the following:

- KEY RESOURCES TABLE
- EXPERIMENTAL MODEL AND STUDY PARTICIPANT DETAILS
  - Strains and growth conditions
  - Bacteriophage lysate preparation
  - Mice
  - Mammalian cell lines
- METHOD DETAILS
  - Strain construction
- DELETION OF THOERIS II SYSTEM IN *P.AERUGINOSA* MRSN11538
- HIGH-THROUGHPUT SCREENING
- EVALUATION OF THOERIS PROTECTION ON SOLID MEDIA
- EVALUATION OF THOERIS PROTECTION IN LIQUID MEDIA
- PHAGE REPRODUCTION MEASUREMENT IN LIQUID MEDIA
- PREPARATION OF PHAGE-INFECTED CELL LYSATE FOR LC-HRMS ANALYSIS
- LC-MS ANALYSIS OF HIS-ADPR, INHIBITOR-ADPR, AND NAD^+ IN THE PHAGE INFECTED-CELL LYSATE
- IP6C-ADPR AND HIS-ADPR PULL-DOWN WITH BaY2ThsB AND $BaY2ThsA^{MACRO}$ PROTEINS
- *IN VITRO* FORMATION OF IP6C-ADPR CATALYZED BY BaY2ThsB AND ArTHSB
- THERMAL SHIFT ASSAY
- LC-MS ANALYSIS OF THE IN VITRO FORMED AND PULLED-DOWN MOLECULES
- PRODUCTION AND PURIFICATION OF $BaY2ThsA^{MACRO}$
- NMR SPECTROSCOPY FOR ENZYMATIC REACTION, STD-NMR, AND IP6C-ADPR STANDARD
- SYNTHESIS AND PURIFICATION OF IP6C-ADPR STANDARD
- *IN VIVO* PHAGE THERAPY EXPERIMENT IN MOUSE MODEL
- MEASURING IMPACT OF IP6C–PHAGE MIXED STORAGE ON LIT1 PHAGE TITER
- HUMAN CELL CULTURE AND CELL VIABILITY ASSAYS
- IP6C SENSITIZATION OF THOERIS-CONTAINING *P. AERUGINOSA* IN A POLYMICROBIAL MODEL CULTURE
- QUANTIFICATION OF IP6C IN A POLYMICROBIAL MODEL CULTURE
- QUANTIFICATION AND STATISTICAL ANALYSIS

SUPPLEMENTAL INFORMATION

Supplemental information can be found online at https://doi.org/10.1016/j.chom.2026.01.003.

Received: July 22, 2025
Revised: November 4, 2025
Accepted: January 2, 2026
Published: January 30, 2026

REFERENCES

1. Murray, C.J.L., Ikuta, K.S., Sharara, F., Swetschinski, L., Robles Aguilar, G., Gray, A., Han, C., Bisignano, C., Rao, P., and Wool, E. (2022). Global burden of bacterial antimicrobial resistance in 2019: a systematic analysis. Lancet *399*, 629–655. https://doi.org/10.1016/S0140-6736(21)02724-0.
2. Hatfull, G.F., Dedrick, R.M., and Schooley, R.T. (2022). Phage Therapy for Antibiotic-Resistant Bacterial Infections. Annu. Rev. Med. *73*, 197–211. https://doi.org/10.1146/annurev-med-080219-122208.
3. Oechslin, F. (2018). Resistance Development to Bacteriophages Occurring during Bacteriophage Therapy. Viruses *10*, 351. https://doi.org/10.3390/v10070351.
4. Georjon, H., and Bernheim, A. (2023). The highly diverse antiphage defence systems of bacteria. Nat. Rev. Microbiol. *21*, 686–700. https://doi.org/10.1038/s41579-023-00934-x.
5. Oromí-Bosch, A., Antani, J.D., and Turner, P.E. (2023). Developing Phage Therapy That Overcomes the Evolution of Bacterial Resistance. Annu. Rev. Virol. *10*, 503–524. https://doi.org/10.1146/annurev-virology-012423-110530.
6. Bleriot, I., Pacios, O., Blasco, L., Fernández-García, L., López, M., Ortiz-Cartagena, C., Barrio-Pujante, A., García-Contreras, R., Pirnay, J.-P., Wood, T.K., et al. (2024). Improving phage therapy by evasion of phage resistance mechanisms. JAC Antimicrob Resist. *6*, dlae017. https://doi.org/10.1093/jacamr/dlae017.
7. Doron, S., Melamed, S., Ofir, G., Leavitt, A., Lopatina, A., Keren, M., Amitai, G., and Sorek, R. (2018). Systematic discovery of antiphage defense systems in the microbial pangenome. Science *359*, eaar4120. https://doi.org/10.1126/science.aar4120.
8. Ofir, G., Herbst, E., Baroz, M., Cohen, D., Millman, A., Doron, S., Tal, N., Malheiro, D.B.A., Malitsky, S., Amitai, G., et al. (2021). Antiviral activity of bacterial TIR domains via immune signalling molecules. Nature *600*, 116–120. https://doi.org/10.1038/s41586-021-04098-7.
9. Roberts, C.G., Fishman, C.B., Zhang, Z., Banh, D.V., Patel, D.J., and Marraffini, L.A. (2025). Bacterial TIR-based immune systems sense phage capsids to initiate defense. Nat. Microbiol. *10*, 2892–2902. https://doi.org/10.1038/s41564-025-02150-0.
10. van den Berg, D.F., Costa, A.R., Esser, J.Q., Stanciu, I., Geissler, J.Q., Zoumaro-Djayoon, A.D., Haas, P.-J., and Brouns, S.J.J. (2024). Bacterial homologs of innate eukaryotic antiviral defenses with anti-phage activity highlight shared evolutionary roots of viral defenses. Cell Host Microbe *32*, 1427–1443.e8. https://doi.org/10.1016/j.chom.2024.07.007.
11. Rousset, F., Osterman, I., Scherf, T., Falkovich, A.H., Leavitt, A., Amitai, G., Shir, S., Malitsky, S., Itkin, M., Savidor, A., et al. (2025). TIR signaling activates caspase-like immunity in bacteria. Science *387*, 510–516. https://doi.org/10.1126/science.adu2262.
12. Sabonis, D., Avraham, C., Chang, R.B., Lu, A., Herbst, E., Silanskas, A., Vilutis, D., Leavitt, A., Yirmiya, E., Toyoda, H.C., et al. (2025). TIR domains produce histidine-ADPR as an immune signal in bacteria. Nature *642*, 467–473. https://doi.org/10.1038/s41586-025-08930-2.
13. Leavitt, A., Yirmiya, E., Amitai, G., Lu, A., Garb, J., Herbst, E., Morehouse, B.R., Hobbs, S.J., Antine, S.P., Sun, Z.J., et al. (2022). Viruses inhibit TIR gcADPR signalling to overcome bacterial defence. Nature *611*, 326–331. https://doi.org/10.1038/s41586-022-05375-9.
14. Manik, M.K., Shi, Y., Li, S., Zaydman, M.A., Damaraju, N., Eastman, S., Smith, T.G., Gu, W., Masic, V., Mosaiab, T., et al. (2022). Cyclic ADP ribose isomers: Production, chemical structures, and immune signaling. Science *377*, eadc8969. https://doi.org/10.1126/science.adc8969.
15. Tamulaitiene, G., Sabonis, D., Sasnauskas, G., Ruksenaite, A., Silanskas, A., Avraham, C., Ofir, G., Sorek, R., Zaremba, M., and Siksnys, V. (2024). Activation of Thoeris antiviral system via SIR2 effector filament assembly. Nature *627*, 431–436. https://doi.org/10.1038/s41586-024-07092-x.
16. Shi, Y., Masic, V., Mosaiab, T., Rajaratman, P., Hartley-Tassell, L., Sorbello, M., Goulart, C.C., Vasquez, E., Mishra, B.P., Holt, S., et al. (2024). Structural characterization of macro domain–containing Thoeris antiphage defense systems. Sci. Adv. *10*, eadn3310. https://doi.org/10.1126/sciadv.adn3310.
17. Storms, Z.J., Teel, M.R., Mercurio, K., and Sauvageau, D. (2020). The Virulence Index: A Metric for Quantitative Analysis of Phage Virulence. Phage (New Rochelle) *1*, 27–36. https://doi.org/10.1089/phage.2019.0001.

18. Essuman, K., Summers, D.W., Sasaki, Y., Mao, X., Yim, A.K.Y., DiAntonio, A., and Milbrandt, J. (2018). TIR Domain Proteins Are an Ancient Family of NAD+-Consuming Enzymes. Curr. Biol. *28*, 421–430.e4. https://doi.org/10.1016/j.cub.2017.12.024.

19. Shi, Y., Kerry, P.S., Nanson, J.D., Bosanac, T., Sasaki, Y., Krauss, R., Saikot, F.K., Adams, S.E., Mosaiab, T., Masic, V., et al. (2022). Structural basis of SARM1 activation, substrate recognition, and inhibition by small molecules. Mol. Cell *82*, 1643–1659.e10. https://doi.org/10.1016/j.molcel.2022.03.007.

20. Bratkowski, M., Burdett, T.C., Danao, J., Wang, X., Mathur, P., Gu, W., Beckstead, J.A., Talreja, S., Yang, Y.-S., Danko, G., et al. (2022). Uncompetitive, adduct-forming SARM1 inhibitors are neuroprotective in preclinical models of nerve injury and disease. Neuron *110*, 3711–3726.e16. https://doi.org/10.1016/j.neuron.2022.08.017.

21. Sabonis, D., Avraham, C., Lu, A., Herbst, E., Silanskas, A., Leavitt, A., Yirmiya, E., Zaremba, M., Amitai, G., Kranzusch, P.J., et al. (2024). TIR domains produce histidine-ADPR conjugates as immune signaling molecules in bacteria. Preprint at bioRxiv. https://doi.org/10.1101/2024.01.03.573942.

22. Neuts, A.-S., Berkhout, H.J., Hartog, A., and Goosen, J.H.M. (2021). Bacteriophage therapy cures a recurrent Enterococcus faecalis infected total hip arthroplasty? A case report. Acta Orthop. *92*, 678–680. https://doi.org/10.1080/17453674.2021.1968714.

23. Köhler, T., Luscher, A., Falconnet, L., Resch, G., McBride, R., Mai, Q.-A., Simonin, J.L., Chanson, M., Maco, B., Galiotto, R., et al. (2023). Personalized aerosolised bacteriophage treatment of a chronic lung infection due to multidrug-resistant Pseudomonas aeruginosa. Nat. Commun. *14*, 3629. https://doi.org/10.1038/s41467-023-39370-z.

24. Lebreton, F., Snesrud, E., Hall, L., Mills, E., Galac, M., Stam, J., Ong, A., Maybank, R., Kwak, Y.I., Johnson, S., et al. (2021). A panel of diverse Pseudomonas aeruginosa clinical isolates for research and development. JAC Antimicrob Resist. *3*, dlab179. https://doi.org/10.1093/jacamr/dlab179.

25. Ceyssens, P.-J., Brabban, A., Rogge, L., Lewis, M.S., Pickard, D., Goulding, D., Dougan, G., Noben, J.-P., Kropinski, A., Kutter, E., et al. (2010). Molecular and physiological analysis of three Pseudomonas aeruginosa phages belonging to the "N4-like viruses". Virology *405*, 26–30. https://doi.org/10.1016/j.virol.2010.06.011.

26. Tomich, P.K., An, F.Y., Damle, S.P., and Clewell, D.B. (1979). Plasmid-Related Transmissibility and Multiple Drug Resistance in *Streptococcus faecalis* subsp. *zymogenes* Strain DS16. Antimicrob. Agents Chemother. *15*, 828–830. https://doi.org/10.1128/aac.15.6.828.

27. Ho, K., Huo, W., Pas, S., Dao, R., and Palmer, K.L. (2018). Loss-of-Function Mutations in *epaR* Confer Resistance to NPV1 Infection in Enterococcus faecalis OG1RF. Antimicrob. Agents Chemother. *62*, e00758-18. https://doi.org/10.1128/AAC.00758-18.

28. Peters, B.M., Jabra-Rizk, M.A., O'May, G.A., Costerton, J.W., and Shirtliff, M.E. (2012). Polymicrobial Interactions: Impact on Pathogenesis and Human Disease. Clin. Microbiol. Rev. *25*, 193–213. https://doi.org/10.1128/cmr.00013-11.

29. Jean-Pierre, F., Hampton, T.H., Schultz, D., Hogan, D.A., Groleau, M.-C., Déziel, E., and O'Toole, G.A. (2023). Community composition shapes microbial-specific phenotypes in a cystic fibrosis polymicrobial model system. eLife *12*, e81604. https://doi.org/10.7554/eLife.81604.

30. Payne, L.J., Todeschini, T.C., Wu, Y., Perry, B.J., Ronson, C.W., Fineran, P.C., Nobrega, F.L., and Jackson, S.A. (2021). Identification and classification of antiviral defence systems in bacteria and archaea with PADLOC reveals new system types. Nucleic Acids Res. *49*, 10868–10878. https://doi.org/10.1093/nar/gkab883.

31. Tesson, F., Hervé, A., Mordret, E., Touchon, M., d'Humières, C., Cury, J., and Bernheim, A. (2022). Systematic and quantitative view of the antiviral arsenal of prokaryotes. Nat. Commun. *13*, 2561. https://doi.org/10.1038/s41467-022-30269-9.

32. Athukoralage, J.S., and White, M.F. (2022). Cyclic Nucleotide Signaling in Phage Defense and Counter-Defense. Annu. Rev. Virol. *9*, 451–468. https://doi.org/10.1146/annurev-virology-100120-010228.

33. Kazlauskiene, M., Kostiuk, G., Venclovas, Č., Tamulaitis, G., and Siksnys, V. (2017). A cyclic oligonucleotide signaling pathway in type III CRISPR-Cas systems. Science *357*, 605–609. https://doi.org/10.1126/science.aao0100.

34. Niewoehner, O., Garcia-Doval, C., Rostøl, J.T., Berk, C., Schwede, F., Bigler, L., Hall, J., Marraffini, L.A., and Jinek, M. (2017). Type III CRISPR–Cas systems produce cyclic oligoadenylate second messengers. Nature *548*, 543–548. https://doi.org/10.1038/nature23467.

35. Stella, G., and Marraffini, L. (2024). Type III CRISPR-Cas: beyond the Cas10 effector complex. Trends Biochem. Sci. *49*, 28–37. https://doi.org/10.1016/j.tibs.2023.10.006.

36. Cohen, D., Melamed, S., Millman, A., Shulman, G., Oppenheimer-Shaanan, Y., Kacen, A., Doron, S., Amitai, G., and Sorek, R. (2019). Cyclic GMP–AMP signalling protects bacteria against viral infection. Nature *574*, 691–695. https://doi.org/10.1038/s41586-019-1605-5.

37. Millman, A., Melamed, S., Amitai, G., and Sorek, R. (2020). Diversity and classification of cyclic-oligonucleotide-based anti-phage signalling systems. Nat. Microbiol. *5*, 1608–1615. https://doi.org/10.1038/s41564-020-0777-y.

38. Tal, N., Morehouse, B.R., Millman, A., Stokar-Avihail, A., Avraham, C., Fedorenko, T., Yirmiya, E., Herbst, E., Brandis, A., Mehlman, T., et al. (2021). Cyclic CMP and cyclic UMP mediate bacterial immunity against phages. Cell *184*, 5728–5739.e16. https://doi.org/10.1016/j.cell.2021.09.031.

39. Loenen, W.A.M., Dryden, D.T.F., Raleigh, E.A., Wilson, G.G., and Murray, N.E. (2013). Highlights of the DNA cutters: a short history of the restriction enzymes. Nucleic Acids Res. *42*, 3–19. https://doi.org/10.1093/nar/gkt990.

40. Hille, F., Richter, H., Wong, S.P., Bratovič, M., Ressel, S., and Charpentier, E. (2018). The Biology of CRISPR-Cas: Backward and Forward. Cell *172*, 1239–1259. https://doi.org/10.1016/j.cell.2017.11.032.

41. Li, J., Cheng, R., Wang, Z., Yuan, W., Xiao, J., Zhao, X., Du, X., Xia, S., Wang, L., Zhu, B., et al. (2024). Structures and activation mechanism of the Gabija anti-phage system. Nature *629*, 467–473. https://doi.org/10.1038/s41586-024-07270-x.

42. Antine, S.P., Johnson, A.G., Mooney, S.E., Leavitt, A., Mayer, M.L., Yirmiya, E., Amitai, G., Sorek, R., and Kranzusch, P.J. (2024). Structural basis of Gabija anti-phage defence and viral immune evasion. Nature *625*, 360–365. https://doi.org/10.1038/s41586-023-06855-2.

43. Tuck, O.T., Adler, B.A., Armbruster, E.G., Lahiri, A., Hu, J.J., Zhou, J., Pogliano, J., and Doudna, J.A. (2024). Hachiman is a genome integrity sensor. Preprint at bioRxiv. https://doi.org/10.1101/2024.02.29.582594.

44. Hu, H., Hughes, T.C.D., Popp, P.F., Roa-Eguiara, A., Martin, F.J.O., Rutbeek, N.R., Hendriks, I.A., Payne, L.J., Yan, Y., Sousa, V.K.D., et al. (2023). Structure and mechanism of Zorya anti-phage defense system. Preprint at bioRxiv. https://doi.org/10.1101/2023.12.18.572097.

45. Arkin, M.R., Tang, Y., and Wells, J.A. (2014). Small-Molecule Inhibitors of Protein-Protein Interactions: Progressing toward the Reality. Chem. Biol. *21*, 1102–1114. https://doi.org/10.1016/j.chembiol.2014.09.001.

46. Radaeva, M., Ton, A.-T., Hsing, M., Ban, F., and Cherkasov, A. (2021). Drugging the 'undruggable'. Therapeutic targeting of protein–DNA interactions with the use of computer-aided drug discovery methods. Drug Discov. Today *26*, 2660–2679. https://doi.org/10.1016/j.drudis.2021.07.018.

47. Maji, B., Gangopadhyay, S.A., Lee, M., Shi, M., Wu, P., Heler, R., Mok, B., Lim, D., Siriwardena, S.U., Paul, B., et al. (2019). A High-Throughput Platform to Identify Small-Molecule Inhibitors of CRISPR-Cas9. Cell *177*, 1067–1079.e19. https://doi.org/10.1016/j.cell.2019.04.009.

48. Lim, D., Zhou, Q., Cox, K.J., Law, B.K., Lee, M., Kokkonda, P., Sreekanth, V., Pergu, R., Chaudhary, S.K., Gangopadhyay, S.A., et al. (2022). A general approach to identify cell-permeable and synthetic anti-CRISPR small molecules. Nat. Cell Biol. *24*, 1766–1775. https://doi.org/10.1038/s41556-022-01005-8.

49. Costa, A.R., van den Berg, D.F., Esser, J.Q., Muralidharan, A., van den Bossche, H., Bonilla, B.E., van der Steen, B.A., Haagsma, A.C., Fluit, A.C., Nobrega, F.L., et al. (2024). Accumulation of defense systems in phage-resistant strains of *Pseudomonas aeruginosa*. Sci. Adv. *10*, eadj0341. https://doi.org/10.1126/sciadv.adj0341.

50. van Houte, S.V., Buckling, A., and Westra, E.R. (2016). Evolutionary Ecology of Prokaryotic Immune Mechanisms. Microbiol. Mol. Biol. Rev. *80*, 745–763. https://doi.org/10.1128/mmbr.00011-16.

51. Puigbò, P., Makarova, K.S., Kristensen, D.M., Wolf, Y.I., and Koonin, E.V. (2017). Reconstruction of the evolution of microbial defense systems. BMC Evol. Biol. *17*, 94. https://doi.org/10.1186/s12862-017-0942-y.

52. Bernheim, A., and Sorek, R. (2020). The pan-immune system of bacteria: antiviral defence as a community resource. Nat. Rev. Microbiol. *18*, 113–119. https://doi.org/10.1038/s41579-019-0278-2.

53. Woo, A.Y.M., Aguilar Ramos, M.A., Narayan, R., Richards-Corke, K.C., Wang, M.L., Sandoval-Espinola, W.J., and Balskus, E.P. (2023). Targeting the human gut microbiome with small-molecule inhibitors. Nat. Rev. Chem. *7*, 319–339. https://doi.org/10.1038/s41570-023-00471-4.

54. Zang, Z., Zhang, C., Park, K.J., Schwartz, D.A., Podicheti, R., Lennon, J.T., and Gerdt, J.P. (2025). Streptomyces secretes a siderophore that sensitizes competitor bacteria to phage infection. Nat. Microbiol. *10*, 362–373. https://doi.org/10.1038/s41564-024-01910-8.

55. Zang, Z., Park, K.J., and Gerdt, J.P. (2022). A metabolite produced by gut microbes represses phage infections in *Vibrio cholerae*. ACS Chem. Biol. *17*, 2396–2403. https://doi.org/10.1021/acschembio.2c00422.

56. Wang, D.-G., Niu, L., Lin, Z.-M., Wang, J.-J., Gao, D.-F., Sui, H.-Y., Li, Y.-Z., and Wu, C. (2021). The Discovery and Biosynthesis of Nicotinic Myxochelins from an Archangium sp. SDU34. J. Nat. Prod. *84*, 2744–2748. https://doi.org/10.1021/acs.jnatprod.1c00524.

57. Frank, N.A., Széles, M., Akone, S.H., Rasheed, S., Hüttel, S., Frewert, S., Hamed, M.M., Herrmann, J., Schuler, S.M.M., Hirsch, A.K.H., et al. (2021). Expanding the Myxochelin Natural Product Family by Nicotinic Acid Containing Congeners. Molecules *26*, 4929. https://doi.org/10.3390/molecules26164929.

58. Wu, Y., Garushyants, S.K., van den Hurk, A., Aparicio-Maldonado, C., Kushwaha, S.K., King, C.M., Ou, Y., Todeschini, T.C., Clokie, M.R.J., Millard, A.D., et al. (2024). Bacterial defense systems exhibit synergistic anti-phage activity. Cell Host Microbe *32*, 557–572.e6. https://doi.org/10.1016/j.chom.2024.01.015.

59. Chatterjee, A., Johnson, C.N., Luong, P., Hullahalli, K., McBride, S.W., Schubert, A.M., Palmer, K.L., Carlson, P.E., and Duerkop, B.A. (2019). Bacteriophage Resistance Alters Antibiotic-Mediated Intestinal Expansion of Enterococci. Infect. Immun. *87*, e00085-19. https://doi.org/10.1128/IAI.00085-19.

60. Huo, W., Adams, H.M., Zhang, M.Q., and Palmer, K.L. (2015). Genome Modification in Enterococcus faecalis OG1RF Assessed by Bisulfite Sequencing and Single-Molecule Real-Time Sequencing. J. Bacteriol. *197*, 1939–1951. https://doi.org/10.1128/jb.00130-15.

61. Yasbin, R.E., Wilson, G.A., and Young, F.E. (1975). Transformation and transfection in lysogenic strains of Bacillus subtilis: evidence for selective induction of prophage in competent cells. J. Bacteriol. *121*, 296–304. https://doi.org/10.1128/jb.121.1.296-304.1975.

62. Guérout-Fleury, A.M., Frandsen, N., and Stragier, P. (1996). Plasmids for ectopic integration in Bacillus subtilis. Gene *180*, 57–61. https://doi.org/10.1016/S0378-1119(96)00404-0.

63. Thurlow, L.R., Thomas, V.C., and Hancock, L.E. (2009). Capsular Polysaccharide Production in *Enterococcus faecalis* and Contribution of CpsF to Capsule Serospecificity. J. Bacteriol. *191*, 6203–6210. https://doi.org/10.1128/jb.00592-09.

64. Choi, K.-H., and Schweizer, H.P. (2006). mini-Tn7 insertion in bacteria with single attTn7 sites: example Pseudomonas aeruginosa. Nat. Protoc. *1*, 153–161. https://doi.org/10.1038/nprot.2006.24.

65. Gibson, D.G., Young, L., Chuang, R.-Y., Venter, J.C., Hutchison, C.A., and Smith, H.O. (2009). Enzymatic assembly of DNA molecules up to several hundred kilobases. Nat. Methods *6*, 343–345. https://doi.org/10.1038/nmeth.1318.

66. Piotto, M., Saudek, V., and Sklenář, V. (1992). Gradient-tailored excitation for single-quantum NMR spectroscopy of aqueous solutions. J. Biomol. NMR *2*, 661–665. https://doi.org/10.1007/BF02192855.

67. Sklenar, V., Piotto, M., Leppik, R., and Saudek, V. (1993). Gradient-Tailored Water Suppression for 1H-15N HSQC Experiments Optimized to Retain Full Sensitivity. J. Magn. Reson., A *102*, 241–245. https://doi.org/10.1006/jmra.1993.1098.

68. Mayer, M., and Meyer, B. (1999). Characterization of Ligand Binding by Saturation Transfer Difference NMR Spectroscopy. Angew. Chem. Int. Ed. Engl. *38*, 1784–1788. https://doi.org/10.1002/(SICI)1521-3773(19990614)38:12<1784::AID-ANIE1784>3.0.CO;2-Q.

69. Loyo, C.L., and Grossman, A.D. (2024). A phage-encoded counter-defense inhibits an NAD-degrading anti-phage defense system. Preprint at bioRxiv. https://doi.org/10.1101/2024.12.23.630042.

70. Le, S., Wei, L., Wang, J., Tian, F., Yang, Q., Zhao, J., Zhong, Z., Liu, J., He, X., Zhong, Q., et al. (2024). Bacteriophage protein Dap1 regulates evasion of antiphage immunity and Pseudomonas aeruginosa virulence impacting phage therapy in mice. Nat. Microbiol. *9*, 1828–1841. https://doi.org/10.1038/s41564-024-01719-5.

71. Li, L., Zhong, Q., Zhao, Y., Bao, J., Liu, B., Zhong, Z., Wang, J., Yang, L., Zhang, T., Cheng, M., et al. (2023). First-in-human application of double-stranded RNA bacteriophage in the treatment of pulmonary Pseudomonas aeruginosa infection. Microb. Biotechnol. *16*, 862–867. https://doi.org/10.1111/1751-7915.14217.

STAR★METHODS

KEY RESOURCES TABLE

REAGENT or RESOURCE	SOURCE	IDENTIFIER
Bacterial and virus strains		
B. subtilis RM125 WT	Bacillus Genetic Stock Center (BGSC)	Cat#1A253
B. subtilis no defense control (RM125, *amyE*::Cam^R)	This study	N/A
B. subtilis BaY2 Thoeris (RM125, *amyE*::BaY2 Thoeris)	This study	N/A
B. subtilis MSX-D12 Thoeris (RM125, *amyE*::BcMSX-D12 Thoeris)	This study	N/A
B. subtilis Pspank (RM125, *amyE*::P_{spank}, Spec^R)	This study	N/A
B. subtilis Pspank-BaY2ThsB (RM125, *amyE*::P_{spank}-BaY2ThsB, Spec^R)	This study	N/A
P. aeruginosa PAO1 no defense control (*aat*Tn7::empty)	This study	N/A
P. aeruginosa PAO1:Thoeris (*aat*Tn7::MRSN11538 Thoeris)	This study	N/A
P. aeruginosa MRSN11538 WT (clinical isolate carrying Thoeris system)	BEI Resources, NIAID, NIH	Cat#NR-51569
P. aeruginosa MRSN11538 ΔThoeris	This study	N/A
E. faecalis OG1RF WT	Lab collection	N/A
E. faecalis DS16 (clinical isolate carrying Thoeris system)	Lab collection	N/A
E. faecalis OG1RF:Thoeris (genomic insertion of P_{bacA}-DS16 Thoeris system in-between OG1RF_11778 and OG1RF_11779)	This study	N/A
S. aureus USA300 (clinical isolate, methicillin-resistant)	Lab collection	N/A
S. sanguinis SK36 (clinical isolate)	American Type Culture Collection (ATCC)	Cat#BAA-1455
SPO1 (*Bacillus* phage)	BGSC	Cat#1P4
Lit1 (*Pseudomonas* phage)	Ceyssens et al.[25]	N/A
NPV1 (*Enterococcus* phage)	Ho et al.[27]	N/A
Chemicals, peptides, and recombinant proteins		
LB broth	VWR	Cat#90003-350
Brain Heart Infusion	Fisher	Cat#DF0037-17-8
Todd-Hewitt broth	Fisher	Cat#DF0492-17-6
Dehydrated Agar	Fisher	Cat#DF0140-07-4
Yeast extract	Fisher	Cat#DF0127-07-1
Casamino acids	Fisher	Cat#DF0231-17-2
Glucose	Sigma Aldrich	Cat#G7528
$(NH_4)_2SO_4$	Sigma Aldrich	Cat#A4418
$MgSO_4$	Sigma Aldrich	Cat#M3634
Spectinomycin	Sigma Aldrich	Cat#S9007
Ampicillin	Sigma Aldrich	Cat#A9518
Chloramphenicol	Sigma Aldrich	Cat#C0378
DMSO	Sigma Aldrich	Cat#D8418
IPTG	Gold Biotechnology	Cat#I2481C50
Formic acid (HPLC)	VWR	Cat#PI85178
K_2HPO_4	Sigma Aldrich	Cat#S5136

(*Continued on next page*)

Continued

REAGENT or RESOURCE	SOURCE	IDENTIFIER
KH_2PO_4	Sigma Aldrich	Cat#S3139
$CaCl_2$	Sigma Aldrich	Cat#C7902
$MgCl_2$	Sigma Aldrich	Cat#63068
Sodium citrate	Sigma Aldrich	Cat# C8532
Lysozyme	Research Products International	Cat#L38100
DpnI	New England Biolab	Cat# R0176
Compound **1**	ChemBridge	Cat#20844368
Compound **2**	ChemBridge	Cat#81552145
Compound **3**	ChemBridge	Cat#60772763
Compound **4** (IP6C)	Combi-Blocks	Cat#QJ-2580
Compound **5**	ChemBridge	Cat#4041017
Compound **6**	Sigma Aldrich	Cat#72340
Compound **7** (Id5C)	Ambeed	Cat#A154365
Compound **8**	Ambeed	Cat#A226558
Compound **9** (nicotinamide)	Ambeed	Cat#A877416
Compound **10**	AstaTech	Cat#O11834
Compound **11**	LabNetwork	Cat#EC15116-87-P1
Compound **12**	Combi-Blocks	Cat#SS-2248
Compound **13**	Ambeed	Cat#A175137
Compound **14**	LabNetwork	Cat#EC15116-81-P1
Compound **15**	LabNetwork	Cat#EC15116-88-P1
Compound **16**	1Click Chemistry	Cat#4C70276
Compound **17**	Ambeed	Cat#A525013
Compound **18**	Combi-Blocks	Cat#QC-9665
Compound **19** (IP6CN)	Combi-Blocks	Cat#QB-9909
Compound **20**	Combi-Blocks	Cat#QB-1389
Compound **21**	Combi-Blocks	Cat#HI-1255
Compound **22**	Combi-Blocks	Cat#ST-7023
Compound **23**	Combi-Blocks	Cat#QY-1211
Compound **24**	Combi-Blocks	Cat#HI-1376
Compound **25**	Combi-Blocks	Cat#SS-5810
Compound **26**	Combi-Blocks	Cat#QA-3929
Compound **29**	Combi-Blocks	Cat#HI-1240
EDCI	Sigma Aldrich	Cat#E7750
DMAP	Sigma Aldrich	Cat#8510550025
HOBt	Sigma Aldrich	Cat#157260
NEt_3	Sigma Aldrich	Cat#TX1200
Dimethylamine	Fisher	Cat#AAH27261AE
4-*tert*-Butylbenzylamine	Sigma Aldrich	Cat#631280
Fetal bovine serum	Midwest Scientific	Cat#USFBS
Bortezomib	MedChemExpress	Cat#HY-10227
Critical commercial assays		
QIAprep Spin Miniprep Kit	QIAGEN	Cat#27104
QIAquick Gel Extraction Kit	QIAGEN	Cat#28704
NEBuilder® HiFi DNA Assembly Master Mix	New England Biolab	Cat#E2621
NEB® 10-beta Electrocompetent *E. coli*	New England Biolab	Cat#C3020K
Q5® Hot Start High-Fidelity 2X Master Mix	New England Biolab	Cat#M0494
Lysing Matrix B	MP Biomedicals	Cat#116911050
Amicon Ultra-0.5 Centrifugal Filter Units 3 kDa	EMD Millipore	Cat#UFC500396
MagStrep® Strep-Tactin®XT beads	IBA	Cat#2-5090-002

(*Continued on next page*)

Continued

REAGENT or RESOURCE	SOURCE	IDENTIFIER
Dynabeads™ His-Tag Isolation and Pulldown beads	Invitrogen	Cat#10103D
Strep-Tactin XT 4flow cartridge	IBA	Cat# 2-5023-001
MycoStrip®	InvivoGen	Cat#rep-mysnc-100
CellTiter-Glo® 2.0 Cell Viability Assay	Promega	Cat#G9241
Phosphate-buffered saline	Sigma Aldrich	Cat#P5493
Pseudomonas Isolation Agar	Difco	Cat#292710
Mannitol Salt Agar	Oxoid	Cat#OXCM085B
Streptococcus Selective Agar	Hardy Diagnostics	Cat#A70
Experimental models: Cell lines		
Human: immortalized retinal pigment epithelial cells (hTERT RPE-1)	ATCC	Cat#CRL-4000
Human: primary dermal fibroblasts normal; neonatal (HDFn)	ATCC	Cat#PCS-201-010
Experimental models: Organisms/strains		
Mouse: BALB/c	Hunan SJA Laboratory Animal Company	RRID:MGI:2161072
Oligonucleotides		
Primers for molecular cloning, see Table S1	This paper	N/A
Recombinant DNA		
pDG1662 (*Bacillus* genomic integration vector at *amyE* locus)	BGSC	Cat#ECE113
pDG1662:BaY2 Thoeris	This study	N/A
pDG1662:BcMSX-D12 Thoeris	This study	N/A
pDR110 (*B, subtilis* genomic integration vector at *amyE* locus, carries P_{spank} promoter)	BGSC	Cat#ECE311
pDR110:BaY2ThsB (P_{spank}-BaY2ThsB)	This study	N/A
pLZ12A (vector carries P_{bacA} promoter for expression in *E. faecalis*)	Chatterjee et al.[59]	N/A
pLZ12A:DS16 Thoeris (P_{bacA}-DS16 Thoeris)	This study	N/A
pWH03 (*E. faecalis* genomic integration vector in-between OG1RF_11778 and OG1RF_11779)	Huo et al.[60]	N/A
pWH03:DS16Ths	This study	N/A
pUC18- Tn7T-LAC empty (*P. aeruginosa* genomic integration vector at *att*Tn7 locus)	This study	N/A
pUC18- mini-Tn7-Thoeris (vector used for generation of *P. aeruginosa* PAO1:Thoeris strain)	Lab collection	N/A
pMQ30_Thoeris (plasmid for knocking out the Thoeris II system in *P. aeruginosa* MRSN11538)	This study	N/A
Software and algorithms		
MassLynx v4.1	Waters Corporation	https://www.waters.com/
PR. Therm Control v2.3.1	NanoTemper Technologies	https://support.nanotempertech.com/hc/en-us/categories/17715896798993-Prometheus
QTOF Acquisition Software vB.02.01 SP1	Agilent Technologies	https://www.agilent.com/
MassHunter vB.05.00	Agilent Technologies	https://www.agilent.com/
TopSpin™ v4	Bruker	https://www.bruker.com/
Mnova v14	Mestrelab Research	https://mestrelab.com
GraphPad Prism v10.4.2	GraphPad Software	https://www.graphpad.com

EXPERIMENTAL MODEL AND STUDY PARTICIPANT DETAILS

Please list here under separate headings all the experimental models/study participants (animals, human participants, plants, microbe strains, cell lines, primary cell cultures) used in the study. For each model, provide information related to their species/strain, genotype, age/developmental stage, sex (and gender, ancestry, race, and ethnicity if reported for human studies), maintenance, and care, including institutional permission and oversight information for the experimental animal/human participant study. The influence (or association) of sex, gender, or both on the results of the study must be reported. In cases where it cannot, authors should discuss this as a limitation to their research's generalizability.

Strains and growth conditions

B. subtilis strains were routinely grown in LB broth at 37 °C or 30 °C and 220 rpm. *E. coli* and *P. aeruginosa* strains were routinely grown in LB broth at 37 °C and 220 rpm. *E. faecalis* strains were routinely grown in Brain Heart Infusion (BHI) broth at 37 °C without agitation. *S. aureus* USA300 was grown as an overnight culture in Tryptic Soy Broth, 37°C, 220 rpm. *S. sanguinis* SK36 was grown as an overnight culture in Tryptic Soy Broth supplemented with 0.5% Yeast Extract, 37°C, 5% CO_2. Please see the specific experimental methods below for further culturing details.

Bacteriophage lysate preparation

To prepare the host culture, an overnight culture of *B. subtilis* pDG1662 was sub-cultured 1:100 into 20 mL LB. The culture was incubated at 37 °C and 220 rpm for 4 hours until the OD_{600nm} reached 0.2. About 1×10^3 plaque forming units (PFUs) of *Bacillus* phage SPO1 were added to the culture. The phage-infected culture was incubated at 37 °C and 220 rpm until bacterial cells were lysed and the culture turned clear. The phage lysate was filtered through a 0.2 μm polyethersulfone filter and stored at 4 °C.

Pseudomonas phage Lit1 was similarly propagated on *P. aeruginosa* PAO1:Tn7 empty, and the host was cultured in LB + 10 mM $MgSO_4$.

Enterococcus phage NPV1 was similarly propagated on *E. faecalis* OG1RF, and the host was cultured in Todd-Hewitt broth (THB) + 10 mM $MgSO_4$.

Mice

Seven-week-old female mice of the BALB/c background were used for the experiments and no animal was excluded from the analyses. The mice were purchased from Hunan SJA Laboratory Animal Company and housed under specific pathogen-free conditions; the housing environment had controlled temperature (20–26 °C), humidity (40–70%) and lighting conditions (12 h light and 12 h dark cycle). The Animal Research Ethics Committee of the Army Medical University reviewed, approved and supervised the protocols for animal research (permit number: AMUWEC20240067).

Mammalian cell lines

Immortalized retinal pigment epithelial cells and primary dermal fibroblasts normal; human, neonatal were obtained from ATCC and maintained in DMEM supplemented with 10% fetal bovine serum (FBS) 100 U/mL penicillin and 100 μg/mL streptomycin at 37 °C with 5% CO_2. Cells were tested for mycoplasma contamination and confirmed negative (InvivoGen MycoStrip).

METHOD DETAILS

Strain construction

Construction of B. subtilis that carry Thoeris systems

The Thoeris cassette with its native promoter from *B. amyloliquefaciens* Y2 [NCBI accession #CP003332, 2071378-2073427 (−)] and *B. cereus* MSX-D12 [NCBI accession #AHEQ01000050, 16453-19685 (+)] were synthesized and cloned into the HindIII site on plasmid pDG1662 by GenScript (Plasmid maps included as Files S1 and S2 in Data S1). The constructed plasmids were propagated in *E. coli* DH5α and selected by 100 μg/mL ampicillin. The plasmids were extracted from *E. coli* DH5a using QIAprep Spin Miniprep Kit. Then the plasmids were transformed into *B. subtilis* RM125 using a protocol adapted from Young et al.,[61] and no defense control strain was generated using pDG1662 empty vector. Briefly, *B. subtilis* RM125 were grown in Medium A (1 g/L yeast extract, 0.2 g/L Casamino acids, 0.5% (w/v) glucose, 15 mM $(NH_4)_2SO_4$, 80 mM K_2HPO_4, 44 mM KH_2PO_4, 3.9 mM sodium citrate, 0.8 mM $MgSO_4$) at 37 °C, 220 rpm until the cessation of logarithmic growth and were allowed to continue growing for another 90 mins. Then *B. subtilis* cells were diluted 10-fold into Medium B (Medium A + 0.5 mM $CaCl_2$ + 2.5 mM $MgCl_2$) and incubated at 37 °C, 300 rpm for 90 mins. 1 μg of plasmid was added to these now-competent cells and incubated at 37 °C, 220 rpm for 30 mins. Transformed *B. subtilis* cells with the double-crossover insertion at the *amyE* locus were selected based on resistance to 5 μg/mL chloramphenicol and sensitivity to 100 μg/mL spectinomycin.[62]

Construction of B. subtilis that expresses BaY2ThsB under IPTG induction

Briefly, BaY2ThsB was placed downstream of the P_{spank} promoter (IPTG-inducible) on plasmid pDR110 and then integrated at the *amyE* locus on *B. subtilis* genome. First, BaY2ThsB was amplified by PCR using pDG1662:BaY2 Thoeris as the template with primers BaY2ThsB_pDR110_F and BaY2ThsB_pDR110_R, followed by DpnI digestion and PCR cleanup using QIAquick PCR Purification Kit. pDR110 was then amplified by PCR using primers pDR110_F and pDR110_R, followed by DpnI digestion and gel purification

using QIAquick Gel Extraction Kit BaY2ThsB was ligated with pDR110 using NEBuilder® HiFi DNA Assembly Master Mix and electroporated into NEB® 10-beta Electrocompetent *E. coli*, which was selected by 100 μg/mL ampicillin. The sequence of the constructed plasmid was verified by whole plasmid sequencing (Plasmid map included as File S3 in Data S1). The plasmid was extracted from *E. coli* NEB® 10-beta using QIAprep Spin MiniPrep Kit before transformation into *B. subtilis* RM125 using the above protocol. Transformed *B. subtilis* cells were selected with resistance to 100 μg/mL spectinomycin. Colonies with double-crossover insertion were verified by colony PCR using primers amyE_F and amyE_R.

All PCR reactions were performed using Q5® Hot Start High-Fidelity 2X Master Mix.

Construction of E. faecalis that carries the Thoeris system

Briefly, the DS16 Thoeris operon was placed downstream of the P_{bacA} promoter (constitutively active) on plasmid pLZ12A, and then the P_{bacA}-DS16 Thoeris cassette was genomically integrated between genes OG1RF_11778 and OG1RF_11779 in *E. faecalis* OG1RF using shuttle vector pWH03.[60] To construct the pLZ12A vector carrying DS16 Thoeris, the genomic DNA of *E. faecalis* DS16 was extracted from 1 mL of overnight culture using Wizard® Genomic DNA Purification Kit (Promega #A1120). The Thoeris operon from the *E. faecalis* DS16 genome [NCBI accession AJEY01000012.1, 80649–82108 (−)] was amplified by PCR using primers DS16_Ths_F and DS16_Ths_R, followed by PCR cleanup using QIAquick PCR Purification Kit. pLZ12A was amplified by PCR using primers pLZ12A_F and pLZ12A_R, followed by DpnI digestion and PCR cleanup using QIAquick PCR Purification Kit. DS16 Thoeris was ligated with pLZ12A using NEBuilder® HiFi DNA Assembly Master Mix and transformed by heat shock into NEB® 5-alpha Competent *E. coli* and selected by 15 μg/mL chloramphenicol. The sequence of the constructed plasmid was verified by whole plasmid sequencing (Plasmid map included as File S4 in Data S1).

To construct the pWH03 vector carrying P_{bacA}-DS16 Thoeris, the P_{bacA} promoter with DS16 Thoeris operon was amplified by PCR using pLZ12A:DS16 Thoeris as the template with primers pLZ12A_DS16Ths_F and pLZ12A_DS16Ths_R, followed by DpnI digestion and gel purification using QIAquick Gel Extraction Kit. The integration vector pWH03 was amplified by PCR using primers pWH03_F and pWH03_R, followed by DpnI digestion and gel purification using QIAquick Gel Extraction Kit. P_{bacA}-DS16 Thoeris was ligated with pWH03 using NEBuilder® HiFi DNA Assembly Master Mix and electroporated into NEB® 10-beta electrocompetent *E. coli* which was selected by 15 μg/mL chloramphenicol. The sequence of the constructed plasmid was verified by whole plasmid sequencing (Plasmid map included as File S5 in Data S1). To generate the P_{bacA}-DS16 Thoeris genomic insertion mutant, pWH03:DS16 Thoeris was electroporated into electro-competent *E. faecalis* OG1RF cells and selected as described previously.[63] The presence of the pWH03:DS16 Thoeris in OG1RF cells was validated by colony PCR using two pairs of primers: pheS_198F and EF2238_200R, EF2238_827F and DS16ThsA_200R. The single-site integration by homologous recombination at either EF2238 or EF2239 was validated by colony PCR using primer pairs OG1RF11777_60F and DS16ThsA_200R or DS16ThsB_321F and OG1RF11780_94R respectively. The genomic integration of P_{bacA}-DS16 Thoeris between EF2238 and EF2239 was validated by colony PCR using primers OG1RF11777_60F and OG1RF11780_94R.

All PCR reactions were performed using Q5® Hot Start High-Fidelity 2X Master Mix.

Construction of P. aeruginosa that carries the Thoeris system

The Thoeris type II locus from Pa MRSN11538 was integrated into the PAO1 genome under regulation of a constitutively active promoter. For chromosomal insertion of Thoeris type II at the Tn7 locus in *P. aeruginosa* PAO1 (PAO1:Thoeris II), the integrating vector pUC18-mini-Tn7T-LAC[64] carrying the Thoeris type II operon was used along with the transposase-expressing helper plasmid pTNS3. The pUC18-mini-Tn7-Thoeris II vector was used for the creation of the PAO1:Thoeris II strain, and the pUC18-Tn7T-LAC empty vector was used for the creation of PAO1:Tn7 empty strain, which was used as a negative control. For insertion of Thoeris II, its operon was PCR amplified from the MRSN11538 *Pa* strain genomic DNA using primers Ths_Pa_11538_F and Ths_Pa_11538_R. The PCR product was gel purified using Monarch DNA gel extraction kit and inserted into the HindIII/BamHI-cleaved pUC18-Tn7T-LAC vector using NEBuilder HiFi DNA Assembly. Next, a constitutively active promoter followed by ribosome binding site was inserted upstream the Thoeris II locus to allow constitutive expression of ThsB and ThsA genes. To obtain this construct, the plasmid from the previous cloning step was PCR amplified using primers pUC18- Tn7_const_Promoter_F and Tn7_const_Promoter_R, followed by DpnI treatment, gel purification, and self-ligation using NEBuilder HiFi DNA Assembly. The resulting plasmids were used to transform into *E. coli* DH5α. The sequence of the constructed plasmid was verified by whole plasmid sequencing (Plasmid map included as File S6 in Data S1). *P.aeruginosa* PAO1 cells were electroporated with the pUC18- mini-Tn7-Thoeris II vector or pUC18-mini-Tn7T-LAC and pTNS3, and the resulting strains were selected on gentamicin-containing plates. Potential integrants were screened by colony PCR. Electrocompetent cell preparations, transformations, integrations, selections, plasmid curing, and FLP-recombinase-mediated marker excision with pFLP were performed as described previously.[64]

DELETION OF THOERIS II SYSTEM IN *P.AERUGINOSA* MRSN11538

Deletion of Thoeris II locus from *P.aeruginosa* MRSN11538 was done through allelic exchange technique. pMQ30_Thoeris II vector carrying sequences flanking the upstream and downstream regions of Thoeris II locus was electroporated to SM10 *E. coli* cells. These cells were conjugated with *P. aeruginosa* MRSN11538. *P. aeruginosa* MRSN11538 cells that acquired the plasmid were selected on VBMM agar supplemented with 50 ug/ml of gentamicin. Next, the colonies were plated on solid NSLB agar containing 15% sucrose and growth overnight at 30°C to promote plasmid loss. The result strains were confirmed by PCR and sequencing.

HIGH-THROUGHPUT SCREENING

The DIVERSet-CL Library Block 1 from ChemBridge was used for the screen. The compounds from the library were prepared as 40 μM in LB + 4% DMSO, and 10 μL of these stock solutions were added into the wells of 384-well plates. An overnight culture of *B. subtilis* Y2 Thoeris was diluted 1:100 into fresh LB media + 5 μg/mL chloramphenicol and incubated at 37 °C, 220 rpm for 2 hours. Then, 20 μL of the freshly grown *B. subtilis* culture was added into each well of 384-well plates, followed by incubation at 37 °C for 1 hour. Then, 10 μL of SPO1 phage in LB (∼1000 PFUs) was added to each well. The plates were incubated at 37 °C in a Biospa8 (Biotek) and the OD_{600nm} in each well was recorded every 1 hour using a Synergy H1 plate reader (Biotek).

The Z-score was calculated by

$$Z\text{-}score = \frac{x - \mu}{\sigma}$$

where:

x is the OD_{600nm} of the well at 10 hours after phage infection,

μ is the mean of OD_{600nm} across the plate at 10 hours after phage infection,

σ is the standard deviation of OD_{600nm} across the plate at 10 hours after phage infection.

EVALUATION OF THOERIS PROTECTION ON SOLID MEDIA

The sensitivity of bacteria hosts to phages on solid media was determined by the small drop plaque assay. In brief, 100 μL of an overnight culture of *B. subtilis* host was mixed in 5 mL 55 °C LB + 0.5% agar and poured on top of an LB + 1.5% agar plate. After the top soft agar layer solidified, 5 μL of 1:10 dilutions of SPO1 in LB was dropped on top of the soft agar. After the phage spot dried, the plate was incubated at 37 °C overnight.

For *P. aeruginosa*, 10 mM $MgSO_4$ was supplemented into LB media, LB + 0.35% agar was used as top agar. 2.5 μL of 1:10 dilutions of Lit1 phage were dropped on top of the soft agar.

For *E. faecalis*, THB media + 10 mM $MgSO_4$ was used for cell growth and phage dilution.

EVALUATION OF THOERIS PROTECTION IN LIQUID MEDIA

The sensitivity of bacteria hosts to phages in liquid media was determined by monitoring the growth curve of bacteria. When testing compounds, compounds were dissolved in DMSO or water depending on their solubility, and 2 μL of these stock solutions were added into wells of a 96-well plate. When not testing compounds, 2 μL of solvent was added into each well. An overnight culture of *B. subtilis* host was diluted 1:100 into fresh LB. Then, 180 μL of the diluted culture of *B. subtilis* was added into wells of 96-well plate. The plate was incubated at 30 °C for 30 mins before 20 μL of SPO1 phage (∼10,000 PFUs) in LB media was added into each well. For no infection control, 20 μL of media was added. The plate was then incubated in a Synergy H1 plate reader (Biotek) at 30 °C, 208 rpm (5 mm orbital shaking) and the growth curve of bacteria was recorded by monitoring OD_{600nm} every 30 min.

For *P. aeruginosa*, the 96-well plate containing compounds was prepared as described above. An overnight culture of *P. aeruginosa* host was diluted 1:100 into fresh LB + 10 mM $MgSO_4$. Then, 180 μL of the diluted culture of *P. aeruginosa* was added into wells of 96-well plate. The plate was incubated at 37 °C for 30 mins before 20 μL of Lit1 phage (∼10,000 PFUs) in LB + 10 mM $MgSO_4$ was added into each well. For no infection control, 20 μL of media was added. The plate was incubated at 37 °C in a Biospa8 (Biotek) and the OD_{600nm} in each well was recorded every 30 min using a Synergy H1 plate reader (Biotek).

For *E. faecalis*, the 96-well plate containing compounds was prepared as described above. An overnight culture of *E. faecalis* host was diluted 1:1000 into fresh THB + 10 mM $MgSO_4$. Then, 180 μL of the diluted culture of *E. faecalis* was added into wells of 96-well plate. The plate was incubated at 37 °C for 1 hour before 20 μL of NPV1 phage (∼1,000 PFUs) in THB + 10 mM $MgSO_4$ was added into each well. For no infection control, 20 μL of media was added. The plate was incubated at 37 °C in a Biospa8 (Biotek) and the OD_{600nm} in each well was recorded every 30 min using a Synergy H1 plate reader (Biotek).

The strength of the Thoeris system under compound treatment was calculated by

$$Thoeris\ strength = \frac{Area(compound) - Area(no\ defense)}{Area(no\ compound) - Area(no\ defense)}$$

where "area" represents the integrated area under the bacterial lysis curve upon phage infection (Figure S2A). The Thoeris strength of the no compound control group was defined as 1, while the Thoeris strength of no defense control was defined as 0.

PHAGE REPRODUCTION MEASUREMENT IN LIQUID MEDIA

Phage reproduction was evaluated by quantifying the number of phages produced after infecting bacterial hosts. When testing compounds, compounds were dissolved in DMSO or water depending on the solubility and 2 μL of these solutions were added into wells of a 96-well plate. When not testing compounds, 2 μL of solvent (DMSO or water) was added into each well. An overnight culture of *B. subtilis* host was diluted 1:100 into fresh LB. Then, 180 μL of the diluted culture of *B. subtilis* was added into the wells

of 96-well plate. The plate was incubated at 30 °C for 30 mins before 20 μL of SPO1 phage (~10,000 PFUs) in LB media was added into each well. The plate was then incubated in a Synergy H1 plate reader (Biotek) at 30 °C, 208 rpm (5 mm orbital shaking) and the growth curve of bacteria was recorded by monitoring OD_{600nm} every 30 min. After 15 hours of incubation, 200 μL of the infected culture was removed and centrifuged at 16,000 g for 10 mins. The PFUs in the supernatant were quantified on *B. subtilis* without defense using the small drop plaque assay described above.

For *P. aeruginosa*, the 96-well plate containing compounds was prepared as described above. An overnight culture of *P. aeruginosa* host was diluted 1:100 into fresh LB + 10 mM $MgSO_4$. Then, 180 μL of the diluted culture of *P. aeruginosa* was added into wells of 96-well plate. The plate was incubated at 37 °C for 30 mins before 20 μL of Lit1 phage (~10,000 PFUs) in LB + 10 mM $MgSO_4$ was added into each well. The plate was incubated at 37 °C in a Biospa8 (Biotek) and the OD_{600nm} in each well was recorded every 30 min using a Synergy H1 plate reader (Biotek). After 15 hours of incubation, 200 μL of the infected culture was removed and centrifuged at 16,000 g for 10 mins. The PFUs in the supernatant were quantified on *P. aeruginosa* without defense using the small drop plaque assay described above.

For *E. faecalis*, the 96-well plate containing compounds was prepared as described above. An overnight culture of *E. faecalis* host was diluted 1:1000 into fresh THB + 10 mM $MgSO_4$. Then, 180 μL of the diluted culture of *E. faecalis* was added into wells of 96-well plate. The plate was incubated at 37 °C for 1 hour before 20 μL of NPV1 phage (~1,000 PFUs) in THB + 10 mM $MgSO_4$ was added into each well. The plate was incubated at 37 °C in a Biospa8 (Biotek) and the OD_{600nm} in each well was recorded every 30 min using a Synergy H1 plate reader (Biotek). After 15 hours incubation, 200 μL of the infected culture was removed and centrifuged at 16,000 g for 10 mins. The PFUs in the supernatant were quantified on *E. faecalis* without defense using the small drop plaque assay described above.

PREPARATION OF PHAGE-INFECTED CELL LYSATE FOR LC-HRMS ANALYSIS

Lysates were prepared as described previously[12] with minor modifications described below. Overnight cultures of *B. subtilis* P_{spank} or *B. subtilis* P_{spank}-Y2 ThsB were diluted 1:100 into 500 mL fresh LB + 100 μg/mL spectinomycin + 1 mM IPTG. When testing inhibitors, 500 μM of the compound was supplemented to the *B. subtilis* P_{spank}-Y2 ThsB culture. The diluted cultures were incubated at 30 °C, 220 rpm for 4 hours until OD_{600nm}~0.3. 50 mL of the culture was removed as a t=0 min sample and immediately centrifuged at 10,000 g at 4 °C for 5 mins. The supernatant was discarded, and the cell pellet was stored at −80 °C. Then, 5 mL of SPO1 phage (~5×10^{10} PFUs/mL) was added to the host cells to reach MOI~10. The infected cell culture was incubated at 30 °C, 220 rpm, and 50 mL of the culture was removed at different time points to be immediately centrifuged at 10,000 g, 4 °C for 5 mins. The supernatant was discarded, and the cell pellet was stored at −80 °C. The cell pellets were thawed at room temperature and resuspended in 600 μL of 100 mM sodium phosphate buffer (pH = 7) + 4 mg/mL lysozyme. After incubation at room temperature for 10 mins, the cells were transferred into 2 ml tubes with Lysing Matrix B and lysed using an Omni Bead Ruptor 12 for 2 × 40 s at 6 m/s with a dwell time of 4 mins in-between. After lysis, the tubes were centrifuged at 15,000 g at 4 °C for 10 mins. Then, 400 μL of each supernatant were transferred to Amicon Ultra-0.5 Centrifugal Filter Units 3 kDa and centrifuged for 45 mins at 14,000 g 4 °C. The filtrate was collected, and 10 μl of each were used for LC-MS analysis.

LC-MS ANALYSIS OF HIS-ADPR, INHIBITOR-ADPR, AND NAD^+ IN THE PHAGE INFECTED-CELL LYSATE

The liquid chromatography analysis was performed on ACQUITY UPLC I-Class PLUS System using a Luna Omega 5 μm Polar C18 100 Å column (250×4.6 mm). The mobile phase A was water + 0.1 % (v/v) formic acid and the mobile phase B was acetonitrile + 0.1 % (v/v) formic acid. The flow rate was kept at 0.7 $mL \cdot min^{-1}$ and the gradient was as follows: 0% B (0–10 min), increase to 2.5% B (10–15 min), increase to 5% B (15–16 min), hold 5% B (16–26 min), increase to 95% B (26–27 min), hold 95% B (27–37 min), decrease to 0% B (37–38 min), hold 0% B (38–48 min). High-resolution electrospray ionization (HR-ESI) mass spectra with collision-induced dissociation (CID) MS/MS were obtained using a Waters Synapt G2S Quadrupole Time-of-Flight (QTOF). The instrument was operated at negative ionization mode. The MS spectra were obtained on the Time-of-Flight analyzer with a scan range of 300–800 Da and analyzed using Masslynx 4.1 software. The *m/z* of interest was filtered through Quadrupole, subjected to CID (energy ramp 34–44 V), and analyzed on the Time-of-Flight analyzer with a scan range of 50–750 Da.

IP6C-ADPR AND HIS-ADPR PULL-DOWN WITH BaY2ThsB AND $BaY2ThsA^{Macro}$ PROTEINS

A 0.4 L culture of *E. coli* TOP10 cells harboring the vector pBAD_DelTM-ThsA-TwinStrep_ThsB-His[12] was induced at OD600 0.6 with 0.2% L-arabinose, IP6C was added to the culture to the final concentration of 1.25 mM and cells were grown overnight at 16 °C. Control cells were induced without the addition of IP6C. The cells were harvested by centrifugation and re-suspended in (1) the Strep-Wash buffer (100 mM Tris-HCl pH 8.0, 150 mM NaCl, 1 mM EDTA, 2 mM phenylmethylsulfonyl fluoride (PMSF)) for $BaY2ThsA^{Macro}$ purification, or (2) His-Wash buffer for (10 mM sodium phosphate pH 8.0, 150 mM NaCl, 0.01% Tween-20, 2 mM PMSF) for BaY2ThsB purification, or (3) 20 mM Tris-HCl pH 8.0 buffer for lysate control, and lysed by sonication. After removing debris by centrifugation, the supernatants were mixed with MagStrep® Strep-Tactin®XT beads for BaY2ThsA purification or Dynabeads™ His-Tag Isolation and pulldown beads for BaY2ThsB purification, accordingly. Protein purification was performed according to manufacturers' protocols. Purified protein was denatured for 5 mins at 98°C and centrifuged for

15 mins at 16,000 *g*. Control lysate was transferred to Amicon Ultra-0.5 Centrifugal Filter Unit 3 kDa and centrifuged for 30 mins at 4°C, 12,000 *g*. Resulting supernatant and filtrate were analyzed by LC-MS (see below).

IN VITRO FORMATION OF IP6C-ADPR CATALYZED BY BaY2ThsB AND ArThsB

To produce IP6C-ADPR in vitro, reactions containing 1 mM NAD^+, 3 mM L-histidine, 10 mM IP6C and 100 μM ThsB were prepared in the reaction buffer containing 10 mM Na-HEPES (pH 7.5 at 25°C), 150 mM NaCl and 5 mM $MgCl_2$ and incubated for 1 day at 25°C and later 6 days at 37°C. Samples were heat-denatured for 5 min at 98°C, centrifuged for 15 min at 16,000 g and the resulting supernatants were analyzed by LC-MS (see below).

THERMAL SHIFT ASSAY

The sample was prepared by mixing BaY2ThsB or ArThsB with IP6C, histidine, or buffer (10 mM HEPES pH = 7.5, 150 mM NaCl, 5 mM $MgCl_2$) in the presence of NAD^+ to a final concentration of 5 μM protein and 1 mM compound. The sample was loaded into capillaries, and 330 nm and 350 nm fluorescence and light scattering were measured in Prometheus NT.48 (NanoTemper) during incubation in temperatures rising at the speed of 0.5 °C min^{-1}. The data were processed using PR. Therm Control software.

LC-MS ANALYSIS OF THE IN VITRO FORMED AND PULLED-DOWN MOLECULES

LC-MS analysis was carried out on 1290 Infinity HPLC system (Agilent Technologies) coupled to a 6520 Accurate Mass Q-TOF LC–MS mass analyzer (Agilent Technologies) with an electrospray ion source. HPLC was carried out on a Supelco Discovery HS C18 column at a temperature of 30 °C. Chromatography was carried out at a 0.3 mL·min^{-1} flow rate using a linear mobile phase gradient over 30 min 0.02% formic acid in water to 0.02% formic acid in acetonitrile. MS was carried out using gas at 300 °C, 10 L·min^{-1} gas flow, 2,500 V capillary voltage, 150 V fragmentator voltage. Data acquisition and analysis were carried out using QTOF Acquisition Software and MassHunter software.

PRODUCTION AND PURIFICATION OF BaY2ThsA^{Macro}

The BaY2ThsA gene were synthesized as a gBlock (Integrated DNA Technologies). BaY2ThsA^{Macro} (residues 83–328) was amplified by polymerase chain reaction and cloned into the pET28b vector using Gibson Assembly reaction.[65] The resulting construct was verified by sequencing. BaY2ThsA^{Macro} in the pET28B vector [C-terminal twin Strep-tag] was produced in *E. coli* BL21 (DE3) cells, using the autoinduction method, and purified to homogeneity, using a combination of Strep-tag affinity chromatography and SEC. Briefly, the cells were grown at 37°C, until an optical density at 600 nm of 0.6 to 0.8 was reached. The temperature was then reduced to 20°C, and the cells were grown overnight for approximately μ hours. The cells were harvested by centrifugation at 5000 *g* at 4°C for 15 min and stored at −80°C. The cell pellets were resuspended in 2 to 3 mL of lysis/wash buffer [20 mM Tris (pH 8.0), 1 M NaCl, 0.5 mM TCEP, 0.1% Triton X-100 and 5% v/v glycerol] per gram of cells. The resuspended cells were lysed using a sonicator and clarified by centrifugation (15,000 *g* for 30 min). The clarified lysate was applied to a Strep-Tactin XT 4flow cartridge pre-equilibrated with 10 CVs of the lysis/wash buffer at a rate of 0.5 mL/min. The column was washed with 10 CVs of the wash buffer, followed by elution of bound proteins using lysis/wash buffer supplemented with 50 mM d-biotin. The elution fractions were analyzed by SDS-PAGE, and the fractions containing the protein of interest were pooled and further purified on a S200 HiLoad 26/600 column pre-equilibrated with gel filtration buffer [20 mM Tris (pH 8.0), 0.5 M NaCl, 0.2 mM TCEP and 5% v/v glycerol]. The peak fractions were analyzed by SDS-PAGE, and the fractions containing BaY2ThsA^{Macro} were pooled and concentrated to final concentrations of approximately 1.6 mg/ml, flash-frozen as 10-μL aliquots in liquid nitrogen, and stored at −80°C.

NMR SPECTROSCOPY FOR ENZYMATIC REACTION, STD-NMR, AND IP6C-ADPR STANDARD

NMR samples were prepared in a total volume of 200 mL consisting of 175 μL HBS buffer (50 mM HEPES, 150 mM NaCl, pH 7.5), 20 μL D_2O, and 5 μL DMSO-d6. Each sample was subsequently transferred to a 3 mm Bruker NMR tube rated for 600 MHz data acquisition. All ^1H NMR spectra were acquired with a Bruker AVANCE NEO 600 MHz NMR spectrometer equipped with quadruple resonance QCIF CryoProbe at 298 K. To suppress resonance from H_2O, a water-suppression pulse program (P3919GP), using a 3-9-19 pulse-sequence with gradients,[66,67] was implemented to acquire spectra with an acquisition delay of 2 s and 32 scans per sample. For enzymatic reaction, ^1H spectra were recorded at multiple time-points depending on instrument availability. The pulse-sequence STDDIFFGP19.3, in-built within the TopSpin™ program (Bruker), was employed to acquire STD-NMR spectra.[68] The on-resonance irradiation was set close to protein resonances at 0.8 ppm, whereas the off-resonance irradiation was set far away from any protein or ligand resonances at 300 ppm. A relaxation delay of 4 s was used, out of which a saturation time of 3 s was used to irradiate the protein with a train of 50 ms Gaussian shaped pulses. The number of scans was 256. All spectra were processed by TopSpin™ 4 and Mnova 14.

SYNTHESIS AND PURIFICATION OF IP6C-ADPR STANDARD

IP6C-ADPR standard was produced via TIR domain catalysed base-exchange using NAD^+ and IP6C as substrates. A 10 mL sample of 0.5 μM His_6-tagged *Bacillus subtilis* SpbK,[69] 5 mM IP6C, and 10 mM NAD^+ in HBS buffer (50 mM HEPES, 150 mM NaCl, pH 7.5) with 2.5% DMSO was incubated at room temperature and reaction progress was monitored intermittently by ^1H NMR over time. To stop the reaction, the His_6-tagged enzyme was removed by incubating the mixture with 200 mL of HisPur™ Ni-NTA resin for 30–60 min. The resin was subsequently removed by centrifugation at 500 x *g* for 1 min and the supernatant was subjected to HPLC-based separation to purify the base-exchange products. A Shimadzu Prominence HPLC equipped with a Synergi™ 4 μm Hydro-RP 80 Å column was used for separation. The mobile phase consisted of phase A (0.04 % (v/v) TFA in water) and phase B (0.04 % (v/v) TFA in acetonitrile). Different gradients, flow rates, and run times were applied depending on prior optimization with individual reaction mixtures. Product peaks were confirmed by comparison with individual chromatograms of NAD^+, nicotinamide, ADPR, and IP6C. Fractions corresponding to the IP6C-ADPR peak were collected, concentrated, lyophilized, and stored at −20°C. NMR characterizations of IP6C-ADPR were performed by the aforementioned NMR spectrometer and the detailed peak assignment can be found in Table S2.

IN VIVO PHAGE THERAPY EXPERIMENT IN MOUSE MODEL

This protocol was adapted from a previous study.[70] Only female mice were used to reduce variability associated with male aggression, stress, and dominance behavior under group-housing conditions. This approach allowed for improved experimental consistency and reduced animal use. Phage Lit1 particles was prepared to exclude other toxins (e.g., LPS) as previously reported.[71]

For the toxicity test of phage and the compounds, 100 μL of Lit1 phage (2×10^8 PFUs) or 50 μL of compound IP6C or Id5C (20 mg/mL) were injected intraperitoneally. Each group included 7 mice, which were observed for 7 days. After 7 days post-infection, mice that survived the initial challenge were euthanized.

For the preliminary phage therapy model experiment presented in the supplemental material, the PAO1:Thoeris strain was cultured in LB at 37 °C until the early stationary phase. Cells were then collected and resuspended in PBS to OD600 of 0.6. A volume of 50 μl (3×10^6 CFUs) of bacteria suspension was intraperitoneally inoculated into 7-week-old BALB/c female mice. Immediately following the bacteria infection, a volume of 50 μl of Lit1 phage (3×10^7) was inoculated intraperitoneally on the other side, followed by the intraperitoneal injection of 80 μl of compound IP6C or Id5C (12.5 mg/mL) at 0h, 12h and 24h after the inoculation of phage. Each group included 7 mice, which were observed for 7 days. After 7 days post-infection, mice that survived the initial challenge were euthanized.

For the final phage therapy model experiment presented in the main text, *P. aeruginosa* MRSN11538 strain was cultured in LB at 37 °C until the early stationary phase. Cells were then collected and resuspended in PBS to OD600 of 0.6. A volume of 100 μL (2×10^6 CFUs) of bacteria suspension was intraperitoneally inoculated into mice. One hour following the bacteria infection, 100 μL mixture of Lit1 phage (2×10^7 PFUs) and compound (10 mg/mL) was injected intraperitoneally on the same side. For the phage only control, 100 μL of Lit1 phage (2×10^7 PFUs) was injected intraperitoneally on the same side after one hour following bacterial infection. For the compound only control, 50 μL of IP6C (20 mg/mL) was injected intraperitoneally on the same side after one hour following bacterial infection. Each group included 7 mice, which were observed for 7 days with body weight measured for each mouse. Food intake was monitored for each group of mice by weighing the remaining chow every 24 h, and fresh chow was added to restore the amount to approximately the initial quantity provided. After 7 days post-infection, mice that survived the initial challenge were euthanized.

MEASURING IMPACT OF IP6C–PHAGE MIXED STORAGE ON LIT1 PHAGE TITER

To six 100 μL replicate dilutions of Lit1 phage lysate in LB media was added either 1 μL DMSO or 1 μL 100 mM IP6C in DMSO (for a final concentration of 1 mM). The initial titer was $\sim10^7$ PFU/mL. All 6 lysates were kept at 4°C for 23 days, after which the phage titers were re-tested by small drop plaque assays.

HUMAN CELL CULTURE AND CELL VIABILITY ASSAYS

Bortezomib was dissolved in DMSO and stored as a 10 mM stock. IP6C and the negative control compound were dissolved in DMSO as 1M stock solutions. Cells were seeded onto 96-well plates at a density of 2,000 cells per well. Twenty-four hours later, media was replaced with 0.1% DMSO (vehicle) or the indicated concentration of compound (six replicate wells per dose). Seventy-two hours later, viability was determined by Promega Cell Titer Glo 2.0 assay. Luminescence values were read on a BioTek Synergy H4 plate reader (Agilent) and data plotted as percent viability relative to DMSO (vehicle) using GraphPad Prism v10.4.2.

IP6C SENSITIZATION OF THOERIS-CONTAINING *P. AERUGINOSA* IN A POLYMICROBIAL MODEL CULTURE

A simplified polymicrobial model was employed based on prior work.[29] Overnight cultures of the three bacteria *S. aureus* USA300 (grown in tryptic Soy Broth, 37°C, 220 rpm), *S. sanguinis* SK36 (grown in tryptic Soy Broth supplemented with 0.5% Yeast Extract, 37°C, 5% CO_2), and *P. aeruginosa* PAO1:Thoeris II (grown in LB, 37°C, 220 rpm) were mixed 1:1:1 and diluted 1:100 into fresh tryptic Soy Broth supplemented with 0.5% Yeast Extract and 10 mM $MgSO_4$. Initial colony-forming units were measured of this mixed

culture by serially diluting in 1× phosphate-buffered saline and plating on Pseudomonas Isolation Agar, Mannitol Salt Agar, and *Streptococcus* Selective Agar. All three were incubated at 37°C (Streptococcus plates with 5% CO_2). 190 μL of each mixture was added to 4 wells of a 96-well plate. Two wells contained 2 μL of DMSO. Two wells contained 2 μL of 30 mM IP6C (final concentration of 300 μM). After mixing, phage Lit1 in 10 μL of LB was added (at MOI of 0.0001) to one well containing DMSO and one well containing IP6C. The other 2 wells were treated with 10 μL LB as a control. After mixing, the 96-well plate was incubated at 37°C in a 5% CO_2 incubator. After 8.5 hours, final colony-forming units were measured for each of the four wells by serially diluting in 1× phosphate-buffered saline and plating on the selective agars stated above. This process was repeated three times to generate three replicates.

QUANTIFICATION OF IP6C IN A POLYMICROBIAL MODEL CULTURE

In the 3 polymicrobial cultures above that contained phage and IP6C, 1 μL of each culture was removed at the start and again after 24 hours of incubation. Each 1 μL sample was immediately added to 1 mL 90% acetonitrile in water. This was diluted 10× further into 90% acetonitrile in water for a total dilution of 10^4. The concentration of IP6C was quantified in all 6 samples by multiple reaction monitoring LC-MS/MS on an Agilent 1290 Infinity II LC coupled to an Agilent 6495C triple quadrupole MS, operating with the Agilent Jet Spray ESI source. An Agilent Poroshell 120 HILICZ 2.1 x 150 mm, 2.7 um particles, passivated with phosphoric acid was used with mobile phases A: 20 mM ammonium acetate buffer, pH 9.2, 5 uM medronic acid and B: 100% acetonitrile. The following gradient was employed (flow rate 0.4 mL/min): 0–1 min, 100% B; 1–8 min, linear gradient to 78% B; 8–12 min, linear gradient to 60% B; 12-15 min, linear gradient to 10% B; 15–18 min, 10% B; 18–19 min, linear gradient to 90% B; 19–22 min, 90% B; 22–23 min, 100% B. For multiple reaction monitoring, two transitions were monitored (quantifier, 162.1→117; qualifier, 162.1→78.1), and concentrations were quantified relative to a calibration curve of pure standard.

Synthesis of compounds 27 and 28

Compounds 27 and 28 were synthesized via the same general strategy (Scheme S1). The ^{1}H NMR spectra were obtained on a Varian 600 MHz Inova NMR spectrometer using Varian/Agilent VnmrJ and Linux workstations. All the spectra were analyzed using Mnova software.

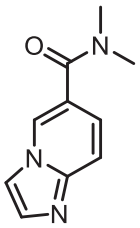

compound **27**

*N,N-dimethylimidazo[1,2-a]pyridine-6-carboxamide (**27**).* Compound **29** (50 mg, 308 μmol), EDCI (65.0 mg, 339 μmol), DMAP (7.5 mg, 62 μmol), NEt_3 (152 mg, 1.5 mmol), and HOBt (45.8 mg, 339 μmol) were added to 20 mL CH_2Cl_2. The mixture was stirred on ice for 1 hour, followed by addition of dimethylamine (27.8 mg, 616 μmol). The reaction mixture was then stirred at room temperature for 18 hours before being washed with 60 mL of saturated Na_2CO_3. The organic layer was dried over anhydrous Na_2SO_4 and concentrated in vacuo. The crude product was purified by silica gel (CH_2Cl_2:MeOH = 20:1) to give compound **27** (20.8 mg, 35% yield) as a pale white solid. ^{1}H NMR (600 MHz, CD_2Cl_2) δ 8.35 (t, *J* = 1.3 Hz, 1H), 7.66 (t, *J* = 1.0 Hz, 1H), 7.63 (d, *J* = 1.3 Hz, 1H), 7.57 (dt, *J* = 9.2, 0.9 Hz, 1H), 7.20 (dd, *J* = 9.2, 1.7 Hz, 1H), 3.05 (s, 6H). Spectrum is shown in Figure S12.

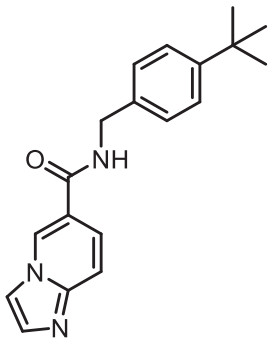

compound **28**

*N-(4-(tert-butyl)benzyl)imidazo[1,2-a]pyridine-6-carboxamide (**28**).* Compound **29** (50 mg, 308 μmol), EDCI (65.0 mg, 339 μmol), DMAP (7.5 mg, 62 μmol), NEt_3 (152 mg, 1.5 mmol), and HOBt (45.8 mg, 339 μmol) were added to 20 mL CH_2Cl_2. The mixture was

stirred on ice for 1 hour, followed by addition of 4-*tert*-butylbenzylamine (100.6 mg, 616 μmol). The reaction mixture was then stirred at room temperature for 18 hours before washed with 60 mL of saturated Na_2CO_3. The organic layer was dried over anhydrous Na_2SO_4 and concentrated in vacuo. The crude product was purified by silica gel (CH_2Cl_2:MeOH = 20:1) to give compound **28** (54.0 mg, 57% yield) as a pale white solid. ^{1}H NMR (600 MHz, CD_2Cl_2) δ 8.83 (t, *J* = 1.4 Hz, 1H), 7.72 (t, *J* = 5.8 Hz, 1H), 7.56 (dd, *J* = 12.2, 1.6 Hz, 2H), 7.51 (dd, *J* = 9.4, 1.8 Hz, 1H), 7.41 (d, *J* = 9.4 Hz, 1H), 7.35 (d, *J* = 8.3 Hz, 2H), 7.27 (d, *J* = 8.2 Hz, 2H), 4.58 (d, *J* = 5.7 Hz, 2H), 1.31 (s, 9H). Spectrum is shown in Figure S12.

QUANTIFICATION AND STATISTICAL ANALYSIS

Data were analyzed and graphed using GraphPad Prism software. Statistical methods are indicated in the figure legends for each experiment in this study.